Journal of Structural Geology 31 (2009) 1490–1510

Contents lists available at ScienceDirect

Journal of Structural Geology

journal homepage: www.elsevier.com/locate/jsg

Fracture-controlled paleohydrology in a map-scale detachment fold: Insights from the analysis of fluid inclusions in calcite and quartz veins

Mark P. Fischer [a,*], I. Camilo Higuera-Díaz [a], Mark A. Evans [b], Eugene C. Perry [a], Liliana Lefticariu [c]

[a] Department of Geology and Environmental Geosciences, Northern Illinois University, DeKalb, IL 60115-2854, United States
[b] Department of Physics and Earth Science, Central Connecticut State University, New Britain, CT 06050-4010, United States
[c] Department of Geology, Southern Illinois University, Carbondale, IL 62901-4304, United States

ARTICLE INFO

Article history:
Received 23 January 2009
Received in revised form
9 September 2009
Accepted 10 September 2009
Available online 17 September 2009

Keywords:
Geofluid
Detachment fold
Vein
Fluid inclusion
Paleohydrology
Mexico

ABSTRACT

This study uses fluid inclusions in quartz and calcite veins to characterize the fracture-controlled paleohydrology of a map-scale, evaporite-cored detachment fold in the Sierra Madre Oriental of northeastern Mexico. Field observations indicate that the veins are tectonic in origin, and that they formed in a general sequence that corresponds to four broad stages of progressive folding. We collected samples from each vein stage in various structural and stratigraphic positions across the fold. After determining the mineral paragenesis and origin of inclusions in each sample, we used standard microthermometric techniques to measure the homogenization temperatures (T_h), salinities and eutectic temperatures of the available two- and three-phase aqueous inclusions. Neither T_h, salinity nor eutectic temperature varied systematically with inclusion origin or mineral type. The data are also not significantly correlated with structural position or vein type, but are strongly partitioned by stratigraphy, suggesting that the area was a vertically stratified hydrologic system consisting of three regional paleohydrostratigraphic units. An upper unit comprised the Indidura Formation through Difunta Group, and is characterized by T_h near 150 °C and salinity <5 wt% NaCl equivalent. A middle unit comprised the Taraises and Cupido Formations, and is characterized by T_h near 150 °C and salinities near 12 or 22 wt% NaCl equivalent. The lower unit comprised the Zuloaga and La Casita Formations, and is characterized by an average T_h near 225 °C and salinities in three groups near 12, 22 or 36 wt% NaCl equivalent. The preservation of multiple, distinct fluid types in many veins suggests that fracture development during folding and uplift created a second paleohydrologic system that overprinted the vertically stratified system. Fracture-controlled fluid migration in this second system occurred in periodic, repeated, and spatially variable pulses.

1. Introduction

Fluids move through and interact with rocks on a variety of time and space scales. The nature of such movements and interactions is controlled by an assortment of stratigraphical, lithological, structural, geochemical and petrological factors that define a complex fluid-rock system. Importantly, the character of such fluid-rock systems continuously evolves as geological processes like burial, diagenesis, and deformation alter the properties of the involved fluids and rocks. Numerous researchers have examined a range of microscopic (e.g. Dieterich et al., 1983; Rye and Bradbury, 1988; Kirschner et al., 1993, 1995), mesoscopic (e.g., Gray et al., 1991; Brantley et al., 1997; Richards et al., 2002), and megascopic fluid-rock systems, the largest of which involve fluid migration across cratonic platforms (e.g. Bethke and Marshak, 1990; Garvin, 1995) or contractional orogenic belts and their adjacent foreland basins (e.g. Dorobek, 1989; Nesbitt and Muehlenbachs, 1994; Evans and Battles, 1999). In the latter case, brittle faults often play a key role in the fluid transport system (e.g. Fyfe and Kerrich, 1985; Vrolijk, 1987; Le Pichon et al., 1992; Sibson, 1996; Janssen, 1998), and may facilitate significant vertical and horizontal fluid migration (e.g. Oliver, 1986; Oliver et al., 1993; Wickham et al., 1993).

In contrast to the numerous studies that have investigated the role of faults in kilometer and larger-scale fluid migration, far fewer studies have examined large-scale fold-related fluid-rock systems (e.g. Cosgrove, 1993; Hanks et al., 2006). The lack of such studies partly reflects the fact that many map-scale folds are in reality fault-related, formed as ramp anticlines above fault bends, or as tip-line folds in front of propagating faults. Consequently, the fluid-rock system of many map-scale folds reflects the combined influences of folding and faulting (e.g., Travé et al., 2000), and the separate contributions of each of these processes are not readily deciphered.

* Corresponding author.
E-mail address: mfischer@niu.edu (M.P. Fischer).

0191-8141/$ – see front matter © 2009 Elsevier Ltd. All rights reserved.
doi:10.1016/j.jsg.2009.09.004

The only place where the specific influence of folding can be determined is in detachment folds, structures that are not cored by substantial, ramping faults.

Detachment folds form when competent layers of rock are folded adjacent to thick sections of weak rocks that are ductally deformed adjacent to a layer-parallel fault, or detachment (e.g. Dahlstrom, 1990; Epard and Groshong, 1995; Homza and Wallace, 1995; Poblet and McClay, 1996; Mitra, 2003). Although some detachment folds do contain faults that cut across stratigraphy (e.g. Rowan, 1997), these faults frequently form late in the folding process, exhibit displacements less than a few tens of meters, and seldom connect to the underlying detachment or adjacent folds (e.g. Mitra, 2003). In the absence of such significant faults to facilitate long distance or cross-stratal fluid transport, the hydrologic structure and migration of fluids in map-scale folds and across fold-dominated orogenic belts is likely to be very different from typical fold and thrust belts (e.g. Evans and Battles, 1999). During detachment folding in particular, fluids most likely migrate through fracture networks that predate or form synchronously with folding (e.g., Jamison, 1997). The history and character of fluid migration should consequently be related to the geometry, spatial distribution and temporal evolution of fractures and fracture connectivity (e.g., Odling et al., 1999).

This paper presents a first-order characterization of the fracture-controlled paleohydrology in a map-scale detachment fold. We begin with a general description of the structural geometry and kinematic evolution of the fold, as well as the timing, stratigraphic distribution, geometry and petrography of vein systems that occur throughout the structure. Fluid compositions, temperatures and sources are interpreted from the analysis of fluid inclusions in quartz and calcite preserved in these veins. Our goal is to define the fluid transport

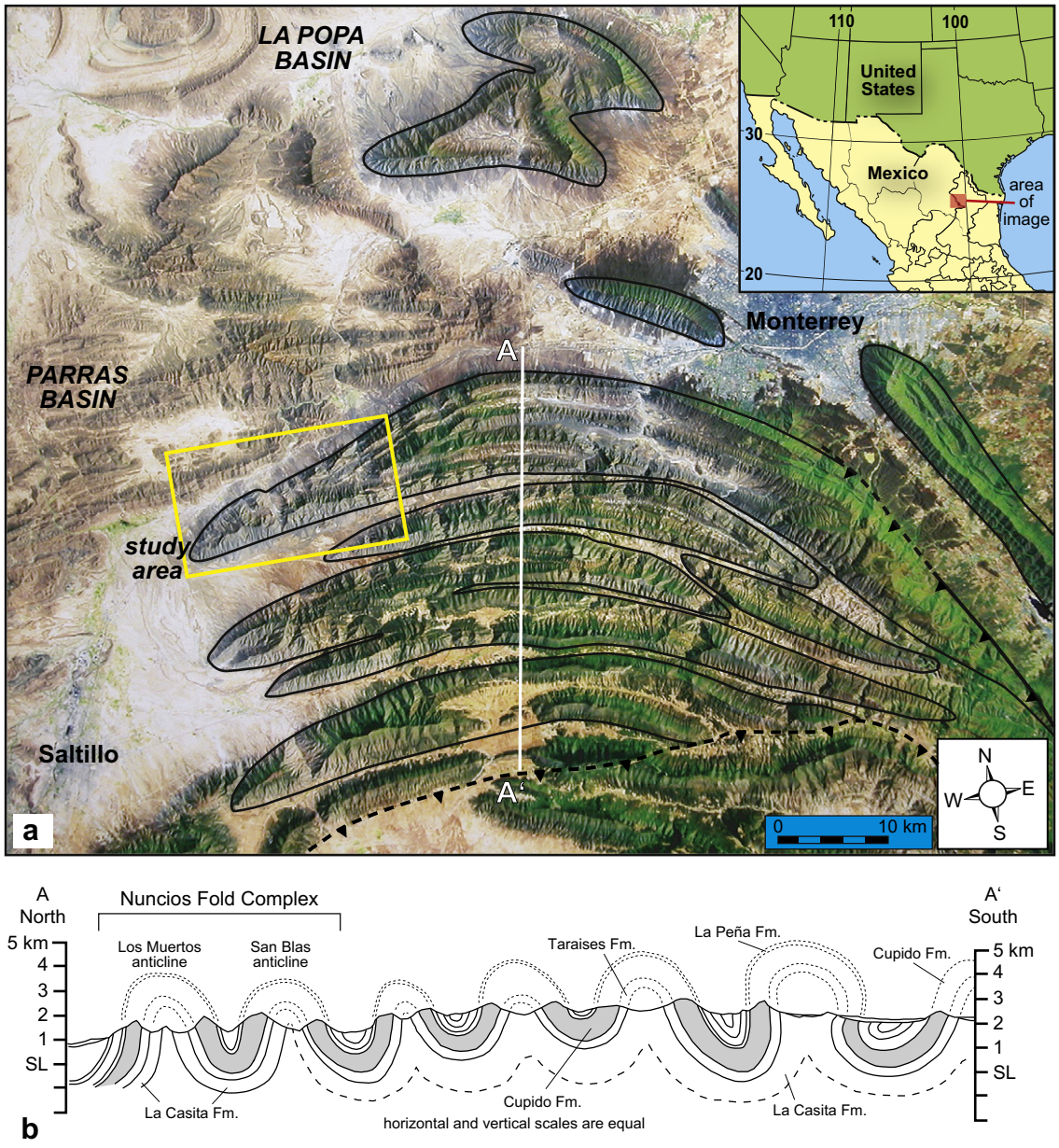

Fig. 1. Regional geological setting. (a) Landsat image of the Monterrey Salient between Monterrey and Saltillo, Mexico. Black line shows the approximate trace of the top of the Aurora/Upper Tamaulipas Formation (Wilson et al., 1984; Goldhammer, 1999) as mapped by Padilla y Sanchez (1982). Note that the scale is approximate and that as presented, north is not aligned with the edge of the image. (b) Regional geological cross-section along the white line in the Landsat image. Modified after Padilla y Sanchez (1982). See Fig. 3 for the regional stratigraphic column.

system, to characterize the fluids that were present, and to interpret how key variables like stratigraphy, structural position and progressive deformation controlled the fluid migration patterns in the fold.

2. Geological setting

The detachment fold we examined is the Nuncios Fold Complex (NFC), the northwesternmost structure in the Monterrey Salient of the Sierra Madre Oriental, a Laramide age orogenic belt that extends throughout most of northern and central Mexico (Fig. 1). This segment of the orogenic belt contains a 3000–5000 m thick sequence of Upper Jurassic and Cretaceous rocks that is detached and folded above a sequence of evaporites that is estimated to have been as much as 1000 m thick prior to the onset of deformation (Wilson et al., 1984; Goldhammer et al., 1991). To the north and west, the Monterrey Salient is bounded by the Parras and La Popa Basins, containing up to an additional 5000 m of latest Cretaceous and Tertiary clastic rocks that are not preserved in the Monterrey Salient (McBride et al., 1974). Because Higuera-Diaz et al. (2005) provided a detailed description of the geology of the NFC, we summarize here only the essential characteristics of the map-scale structural geology and the involved stratigraphy.

Fig. 2 shows that the NFC consists of three folds that interfere, merge, and ultimately terminate toward the west. Los Muertos and San Blas anticlines plunge gently westward while the intervening Sierra Urbano syncline plunges gently eastward. All three folds are clearly distinguished along the eastern edge of the study area where they comprise a composite, upright, symmetric structure with vertical limbs (section C–C′ of Fig. 2). Toward the west this composite fold gradually transforms into a single, asymmetric, north-vergent anticline with a subvertical forelimb and moderately dipping backlimb (section A–A′ of Fig. 2). The entire structure is detached above evaporites of the Minas Viejas Formation (Fig. 3), which is locally extruded through the crest of the anticline, and is interpreted to form a 1–2 km high "wall" beneath the core of the fold (Higuera-Diaz et al., 2005). Although only exposed in one or two localities in the fold belt,

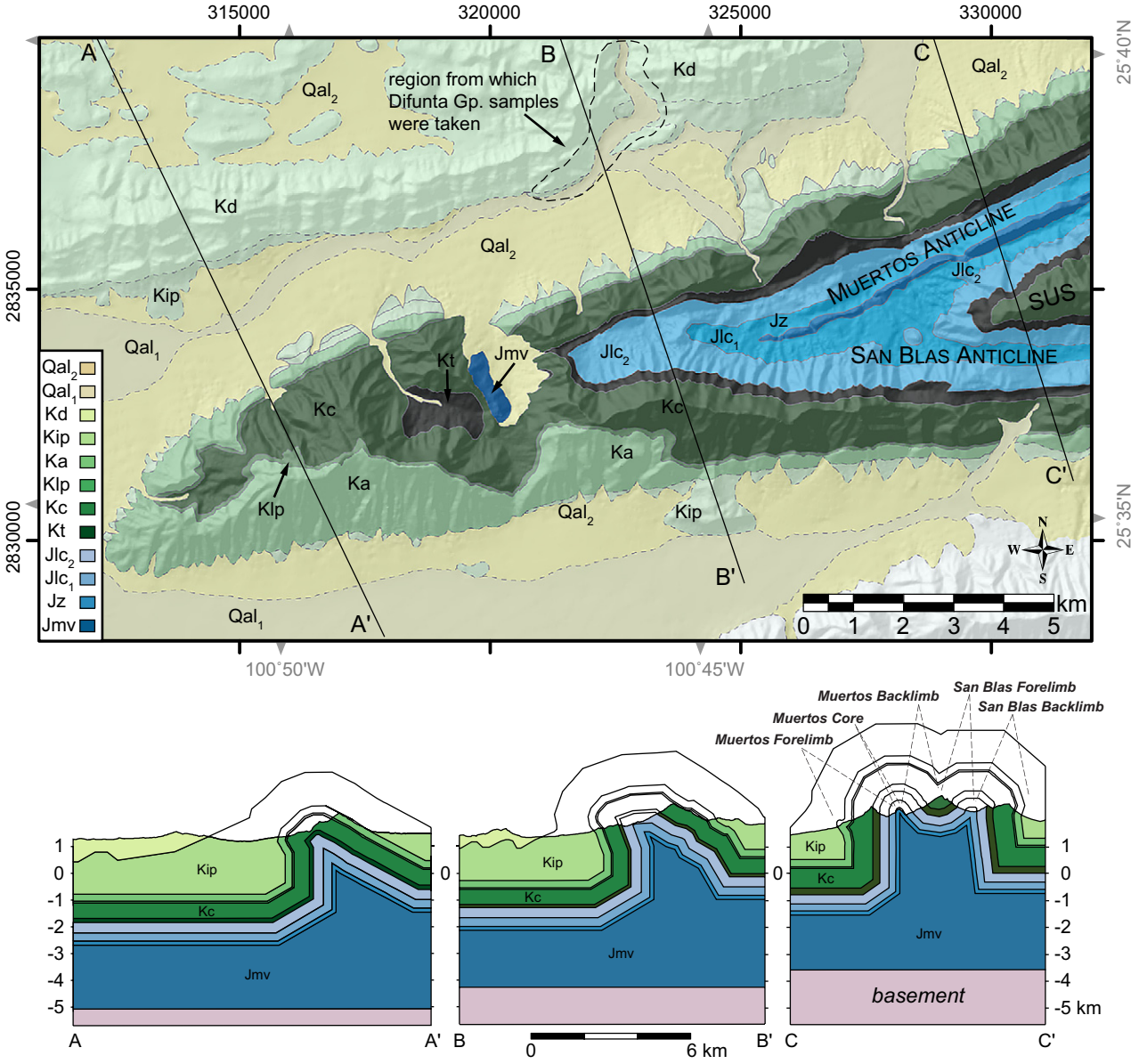

Fig. 2. Geological map and cross sections through the Nuncios Fold Complex. See Fig. 3 for the regional stratigraphic column and associated map symbols. SUS = Sierra Urbano syncline. Modified after Higuera-Diaz et al. (2005).

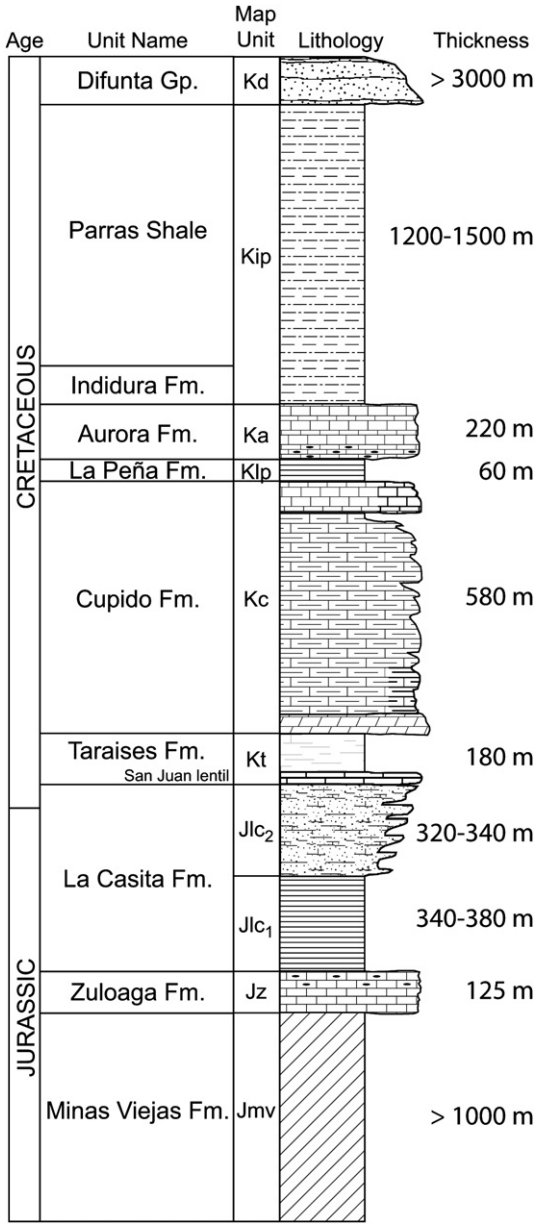

Fig. 3. Generalized stratigraphic column for the area surrounding the Nuncios Fold Complex. Map units and symbols are those shown in Fig. 2. Modified after Higuera-Diaz et al. (2005).

the Minas Viejas detachment layer is widely interpreted to underlie all of the Monterrey Salient and a significant portion of La Popa Basin to the north (e.g., Wall et al., 1961; Marrett and Aranda-Garcia, 1999), where it crops out as diapirs and has been penetrated by exploration wells (Wall et al., 1961; Weidie and Martinez, 1970; Laudon, 1984; Giles and Lawton, 1999).

Above the Minas Viejas Formation, eight additional Jurassic–Cretaceous lithostratigraphic units are involved in the NFC or are exposed in the adjacent Parras Basin (Fig. 3). An incomplete section of the Zuloaga Formation is exposed above the Minas Viejas Formation, and is primarily thick-bedded, gray wackestones with occasional calcareous, gray mudstones and black chert. The La Casita Formation overlies the Zuloaga Formation and consists of a lower, predominantly black shale and siltstone interval that grades upward into an equally thick section of coarsening upward sequences of black shale, lithic sandstone, conglomerate and fossiliferous packstone. Higuera-Diaz (2005) mapped and informally named these two parts of the formation the La Casita 1 and La Casita 2 (Fig. 2). Overlying these units is the Taraises Formation, comprising an upper section of calcareous mudstone and shale and a lower section of extremely well-indurated, fossiliferous packstone and wackestone informally named the San Juan lentil. Above the Taraises Formation is the Cupido Formation, a thick section of carbonates with a massive, bioclastic, dolomitic base, a well-bedded, medium- to thick-bedded middle interval of cyclic, shallowing-upward parasequences of limestone and lesser dolostone, and an upper section of well-bedded, thin- to medium-bedded mudstone, packstone and wackestone. A thin section of calcareous black shale and rare thin-bedded, cherty wackestone overlies the Cupido Formation, and comprises the La Peña Formation. This formation is overlain by the Aurora Formation, which consists of well-bedded wackestone and calcareous mudstone with local black chert near the base. Overlying the Aurora Formation is the Indidura Formation, comprising medium-bedded to laminated dark gray wackestone and packstone that alternates with calcareous shale, brown wackestone and gypsum laminae. Above the Indidura Formation are the Parras Shale and the Difunta Group, two thick clastic sections that only crop out in the Parras Basin, on the northern side of the NFC. The Parras Shale is almost entirely black to gray shale with minor intervals of limestone and gypsum, whereas the Difunta Group consists of fine-grained quartz sandstones with intervals of red beds and limestone.

3. Characteristics of vein systems in the Nuncios Fold Complex

We observed thousands of veins in the ~200 km^2 region and ~3 km thick stratigraphic section comprising the NFC. Although veins are present in all lithostratigraphic units in the region, their abundance, distribution, and morphology are variable. In contrast, the petrology and paragenesis of the veins is remarkably simple and generally consistent. Calcite is the predominant mineral in nearly every sampled vein and usually accounts for >95% of vein volume in carbonate units throughout the area. In addition to calcite, veins in siliciclastic units commonly contain 10–40% quartz, and some are almost exclusively quartz.

Because there is no single location where all types of veins occur together, it was impossible to use cross-cutting relationships to unequivocally determine the timing of all the veins we examined. Lacking such precise constraints, we instead established the relative timing of veins by interpreting their origin with respect to the kinematic history of folding. In this manner, we defined four stages of regional vein formation (Fig. 4). Although veins from each of these stages may have different morphology and mineralogy in different stratigraphic units and widely separated outcrops, their kinematic and strain significance with respect to folding is everywhere consistent. Local cross-cutting relations between the one or two vein sets commonly seen at any single outcrop are consistent with our interpreted sequence of regional vein formation.

In the following sections we describe the field characteristics, stratigraphic distribution, interpreted kinematic significance, mineralogy and paragenesis of veins formed during each of the four stages of fracturing in the NFC. Greater details are provided by Fischer and Jackson (1999) and Higuera-Diaz (2005). Marrett and Laubach (2001), Monroy-Santiago et al. (2001) and Ortega and Marrett (2001) also discuss the origin and characteristics of veins in the Sierra Madre Oriental, but these studies only examined fractures in the Cupido Formation, primarily in different map-scale folds at outcrops located tens of kilometers from our study area. In addition, these studies focused on veins in dolostones that formed in association with boudin necks, solution-collapse breccias and slumps that Marrett and Laubach (2001) interpret as non-tectonic. None of these veins are included in this study.

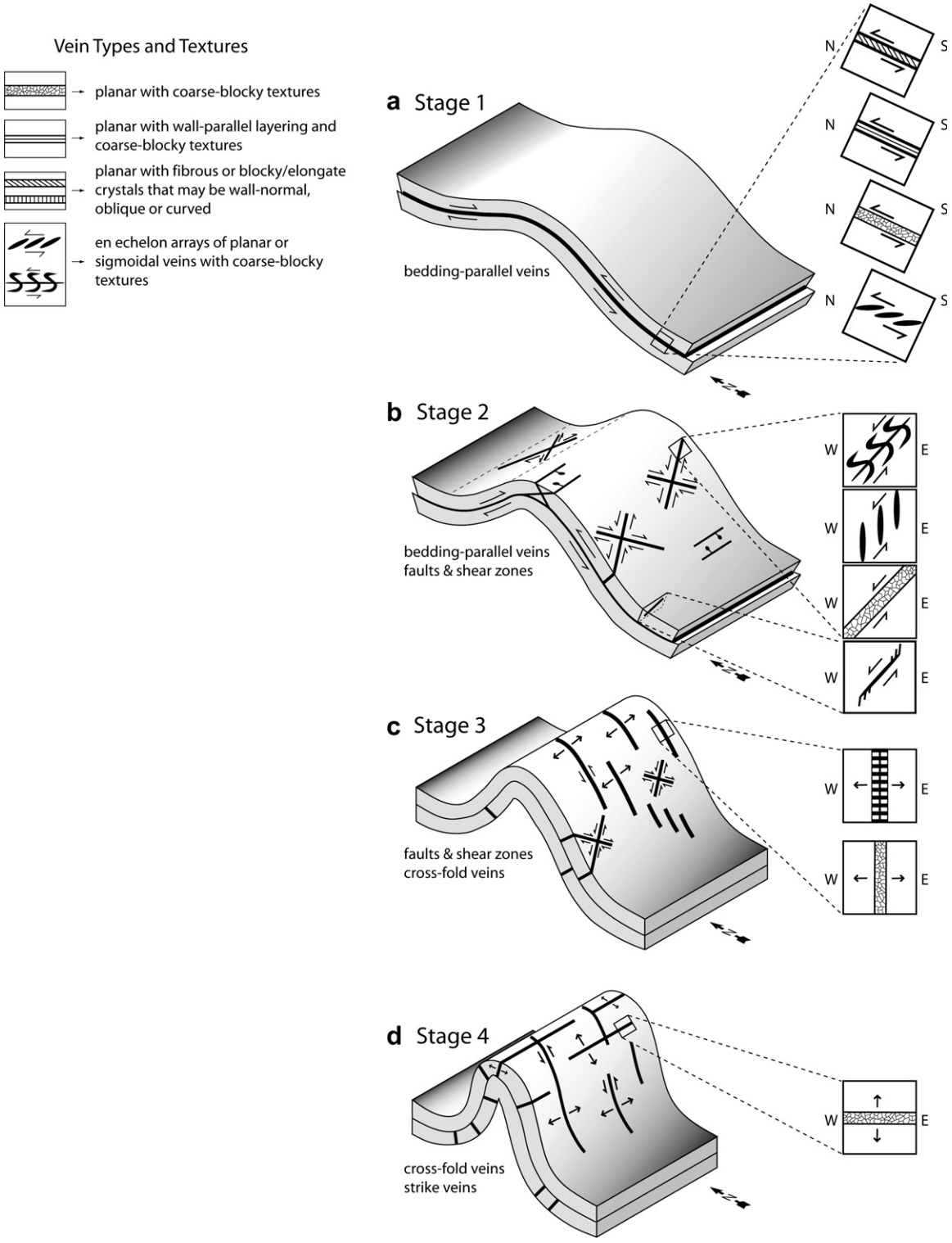

Fig. 4. Sequential stages of fracturing during creation of the Nuncios Fold Complex. (a) Early flexural slip and flow is accommodated by bedding-parallel veins of four main types. (b) Early to intermediate axis-normal shortening is accompanied by hinge-parallel and down-dip extension. This deformation is accommodated by planar, stratabound faults with pinnate tails, shear zones, and en echelon vein arrays. Bed-parallel veins also continue to form during this time. (c) Intermediate to late hinge-parallel extension and fold flattening begins to be accommodated by planar cross-fold veins. Faults and shear zones like those in stage 2 continue to form during this time, and some cross-fold veins are reactivated in shear. (d) Intermediate to late outer arc extension or elastic relaxation during uplift is accommodated by localized, rare, axis-parallel strike veins. Cross-fold veins also continue to form during this time. Some early-formed cross-fold veins are reactivated in shear.

3.1. Stage 1 veins

Veins that formed during this stage of folding were seen in all stratigraphic units except the San Juan lentil of the Taraises Formation (Fig. 3). Cross-cutting relations consistently show that when present, these veins are always the oldest structures in any particular outcrop. We interpret that these veins formed during the early to intermediate stages of folding, when increasing limb dips would have resulted in

increasing resolved shear stresses between layers. Four general types of such flexural-slip veins are widespread in the NFC (Fig. 4a). Three of these are planar veins oriented parallel to bedding or an early tectonic foliation that is subparallel to bedding. These planar veins vary in thickness from 2 to 25 cm, and may have sparry, fibrous or layered textures (Fig. 5a). The walls of these veins are locally decorated with slickenlines that are oriented subnormal to the regional fold axis and down the dip of bedding. The sense of shear in these veins is always up dip of local bedding and top toward the regional anticlinal hinges. The layered textures most likely formed as a result of multiple, repeated slip and opening events. The fourth type of flexural-slip vein consists of en echelon segments arranged in geometries that are also consistent with a top toward the anticlinal hinge sense of shear (Fig. 4a). Regardless of host rock composition, flexural-slip veins in the NFC may be comprised of calcite or calcite and quartz.

Stage 1 veins are rare in the Aurora, La Peña and Cupido Formations and are >99% calcite. In our limited suite of samples for these units, petrographic analysis indicates that the calcite was precipitated in a single generation in all these units except the Cupido, which locally contains two or three generations of calcite fill that are distinguished by variations in color, cloudiness, twining or stable isotopic composition (Lefticariu et al., 2005). Stage 1 veins in the Difunta Group contain up to 10% quartz that either post-dates or was co-precipitated with calcite. Minor amounts of later quartz are also present in stage 1 veins in the Zuloaga Formation, some of which also contain a second generation of untwined or cloudy calcite or early dolomite. In the Taraises and La Casita Formations, stage 1 veins are comprised of up to 50% quartz but the relative proportions of quartz and calcite are highly variable from sample to sample. Although calcite is early and present in all stage 1 veins from these units (Fig. 6a), some veins contained a second generation of calcite or two generations of quartz. Many samples showed evidence for significant co-precipitation of calcite and quartz (Fig. 6b).

3.2. Stage 2 veins

Veins that formed during this stage of folding were seen in all stratigraphic units except the Aurora and La Peña Formations (Fig. 3). They are frequently restricted to individual beds, and are best developed in the most competent rocks in the stratigraphic section: arkosic sandstones in the La Casita 2, and dolomitic limestones in the lower Cupido Formation. Veins that form during folding stage 2 overlap in time with veins of stage 3, and occur in one of four main types, each of which extends bedding in a direction parallel to the bearing of the regional fold axis or down the dip of local bedding (Fig. 4b). The four types are planar faults, isolated or paired arrays of straight, en echelon veins (Fig. 5b), arrays of sigmoidal veins with throughgoing fault cores, and isolated faults with pinnate tails. The aperture of stage two veins typically varies from 1 to 3 cm, and they are most often comprised of sparry or elongate blocky calcite with subordinate amounts of quartz.

Stage 2 veins in all units contain greater proportions of quartz than stage 1 veins. Although early calcite is still consistently followed by quartz precipitation (Fig. 6c), quartz routinely accounts for 10–20% of the volume of stage 2 veins in all units. The relative proportions of quartz and calcite are highly variable between veins, and many veins show evidence for a period of co-precipitation between quartz and calcite, as well as two generations of either calcite or quartz (Fig. 6d). Second generation fillings are most prevalent in the La Casita and Cupido Formations, with veins in the latter unit locally containing three generations of calcite, each displaying a characteristic stable isotopic signature or color (e.g., Lefticariu et al., 2005). Early dolomite is present in some stage 2 veins in the Cupido Formation, but this is rare. Stage 2 veins in the Zuloaga Formation and San Juan lentil of the Taraises Formation are unique in that they contain <1% quartz.

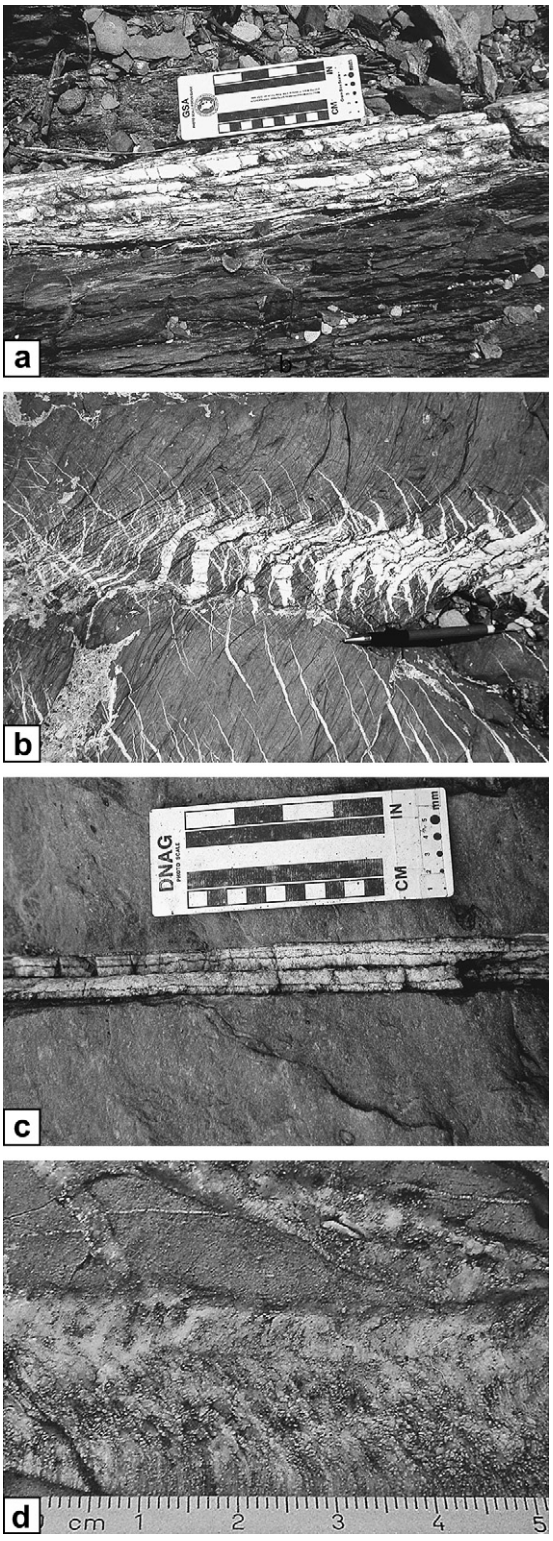

Fig. 5. Examples of typical veins exposed in the study area. (a) Planar, bed-parallel vein with wall-parallel layering and a coarse, blocky texture within individual vein layers. This stage 1 vein is comprised of quartz and calcite and is exposed in the La Casita 1. (b) En echelon array of sigmoidal calcite veins with coarse, blocky texture. This stage 2 vein array is exposed in the lower Cupido Formation. (c) Planar, cross-fold calcite vein with wall-parallel laminations, a fibrous/blocky-elongate texture and wall-normal fibers. This stage 3 vein is exposed in the La Casita 2. (d) Planar fault comprised of calcite fibers that are normal to the vein wall at the vein edges, but oblique to the vein wall near the vein center. This stage 2 vein is exposed in the Cupido Formation.

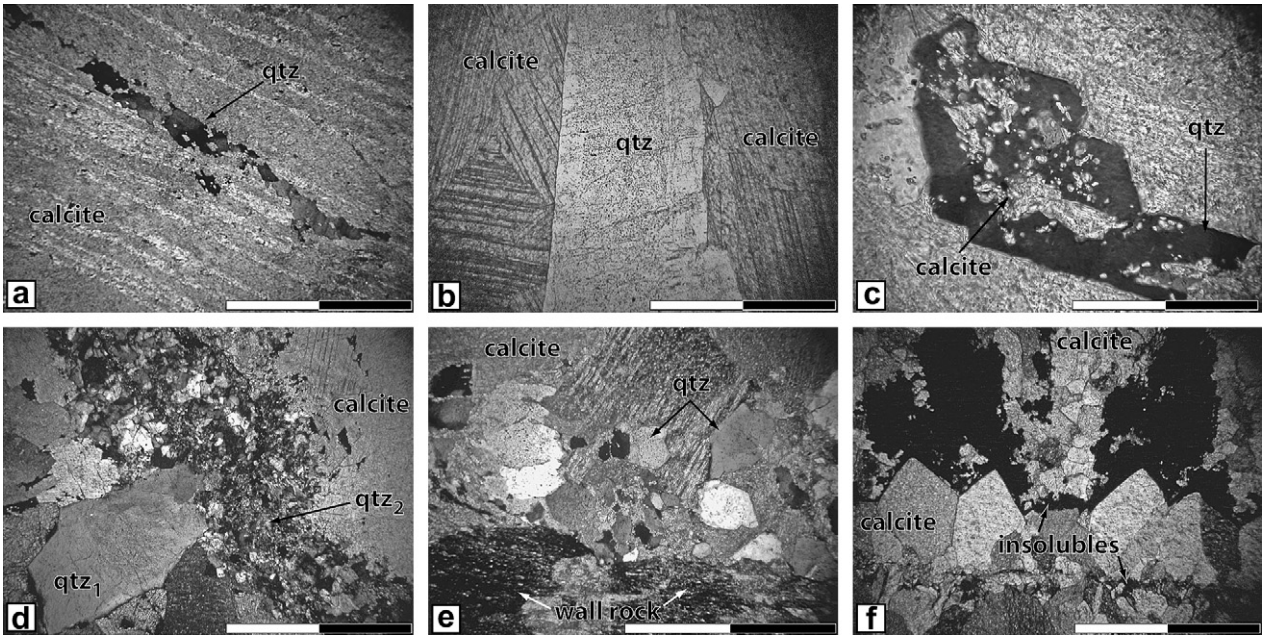

Fig. 6. Example photomicrographs illustrating common paragenetic relations and petrographic textures in veins from the study area. (a) Polarized light view of later quartz replacing twinned calcite in a stage 1 bedding-parallel vein from the La Casita 1. (b) Plane light view of intergrown blocky-elongate calcite and quartz crystals in a stage 3 cross-fold vein in the Difunta Group. (c) Polarized light view of calcite fragments preserved in a well-formed quartz crystal in a stage 2 fault in the La Casita 2. (d) Polarized light view of two generations of quartz in a stage 2 shear zone in the Cupido Formation. Sparry crystals of early calcite and quartz are cut by later, finely crystalline quartz in an irregular zone with concentrated iron oxides and clays(?). (e) Polarized light view of co-precipitated(?) calcite and quartz in a stage 1 vein from the Taraises Formation. Evidence for co-precipitation comes from lack of calcite fragments in quartz, straight grain boundaries between calcite and quartz, prevalence of quartz at boundaries of calcite crystals. (f) Polarized light view of calcite in a stage 3 cross-fold vein in the La Casita 1. Concentrated insolubles (clays, Fe-oxides?) on two sides of well-formed crystals are indicative of multiple opening and closing events that were separated by periods of dissolution. Scale bar is 1 mm long in all images.

3.3. Stage 3 veins

Veins that formed during this stage of folding were observed in all stratigraphic units except the La Peña and Taraises Formations (Fig. 3). These veins are usually vertical, planar, cross-fold fractures that in limestones and dolostones are confined to individual beds, but in shales may cut through several meters of stratigraphy (Fig. 4c). Cross-cutting relations consistently show that stage 3 cross-fold veins postdate stage 1 veins and overlap slightly in time with stage 2 veins. They range in thickness from 2 to 10 cm, with the thickest veins occurring in layers with coarser grains. The mineralogy of these veins appears linked to the composition of the host rock, such that veins in carbonate units contain only calcite, veins in clastic–carbonate units contain both calcite and quartz, and occasionally, in siliciclastic rock, the veins contain only quartz. Irrespective of mineralogy, the textures of stage three cross-fold veins may be fibrous, elongate blocky or sparry, and many veins exhibit a strong wall-parallel color banding that suggests multiple episodes of opening (Fig. 5c). Abrupt textural changes occur across planar boundaries between elongate blocky and sparry crystals, and also suggest separate, distinct episodes of mineralization. Kinematic indicators and displaced markers along many longer cross-fold veins show a consistent east-side-north sense of motion that we interpret as a later reactivation of what were initially cross-fold joints. Our interpretation is based on the extreme planarity and lateral continuity of the fractures, the curvature of fibers in some veins, and the fact that many cross-fold veins show an early stage of sparry filling followed by a later stage of elongate blocky filling that is oblique to the vein walls.

Stage 3 veins show paragenetic relations that are similar to those of stage 1 veins. In the Difunta Group, Aurora, Cupido, and Zuloaga Formations, stage 3 veins typically contain >95% calcite that was precipitated as a single generation and followed by minor amounts of quartz. Some veins in the Taraises Formation show evidence for a late-stage period of calcite and quartz co-precipitation (Fig. 6e). In comparison, stage 3 veins in the La Casita Formation show inconsistent paragenesis and may contain 85–95% quartz or >95% calcite. Although these veins are most commonly comprised of intergrown and co-precipitated crystals of quartz and calcite, calcite appears to have preceded quartz in veins that are predominantly comprised of calcite, and quartz appears to have preceded calcite in veins comprised of mostly quartz. Irrespective of paragenesis, many stage 3 veins in the La Casita contain wall-rock inclusion bands, wall-parallel color banding or wall-parallel bands of insolubles that together suggest that these veins were the product of multiple opening events (Fig. 6f).

3.4. Stage 4 veins

Veins that formed during the latest stages of folding strike parallel to the trend of the regional fold axis, and were observed only in Difunta Group rocks of the foreland, or in rocks of the La Casita and Zuloaga Formations exposed in the hinge zones of the Muertos and San Blas anticlines (Figs. 2 and 3). In the hinge zone regions these veins are 10–20 cm thick, at least 2 m long, planar fractures that are subperpendicular to bedding and comprised of massive calcite. Near the Minas Viejas gypsum/anhydrite intrusion in the center of the map area, these veins can be as thick as 1 m, and often contain calcite plus iron oxides and lead mineralizations. We interpret that these veins formed during fold tightening, outer arc stretching and concomitant upward intrusion of evaporites in the fold core (Fig. 4d). As such, they accommodate fold-axis perpendicular extension of the anticlinal crests. In contrast, stage 4 veins in the foreland are 1–2 cm wide, planar, calcite and quartz veins that commonly occur in thicker, well-indurated sandstone beds. These

veins are uncommon, but were most often seen in the hinge zones of minor, close to open folds with kilometer scale wavelengths. We interpret that these veins formed either by outer arc stretching, or by thermoelastic expansion during uplift.

Stage 4 veins are uncommon throughout the map area and are only represented by one sample from the Difunta Group. This vein contains ≥90% early calcite with <10% later quartz that locally replaces calcite.

3.5. Sampling methodology

Our sampling strategy was guided by our goal of describing the paleohydrology of the NFC on a scale of hundreds of meters to several kilometers. Where possible, we collected at least two samples of each vein type exposed in each lithostratigraphic unit in each of the five structural domains comprising the fold complex (Fig. 2). Most of the samples were collected within 2–3 km of cross section C–C′ along the eastern edge of the map area (Fig. 2). So that we might distinguish the paleohydrology of the fold belt from that of the adjacent Parras Basin, we also collected at least two samples of each vein type found in lower Difunta Group rocks exposed along a major drainageway in the north-central portion of the map area (Fig. 2). In total, we collected roughly 100 vein samples. The specific location of each sampling station is shown on the map provided in the supplementary data accompanying this article.

4. Fluid inclusion analysis

Our philosophy for analyzing the inclusions followed our field approach to interpreting the veins. The goal was to document the regional characteristics of fluids that were present in different parts of the stratigraphic section, in different structural positions on the fold, or during different periods of geological time, each related to a certain stage of vein formation and a corresponding phase of the progressive folding history. In each sample we first surveyed the available inclusions and classified them according to their composition, morphology and host mineral. We distinguished three types of fluid inclusions in our samples: two-phase aqueous inclusions (Fig. 7a), three-phase inclusions containing an aqueous fluid, a vapor bubble, and a halite cube (Fig. 7b), and single-phase inclusions (Fig. 7c). Two-phase aqueous inclusions are the most common type of inclusion found in our samples, occurring in all vein stages in every stratigraphic level examined. They are colorless at room temperature, <2 to >50 μm along the maximum dimension, and have liquid:vapor ratios of 95:5 to 90:10. Three-phase aqueous inclusions occur primarily in veins from the La Casita Formation. They are colorless at room temperature, <2 to >150 μm along the maximum dimension, have liquid:vapor ratios of 95:5 to 90:10, and contain a halite cube with approximately the same volume as the vapor bubble. The single-phase inclusions are colorless, monophase at room temperature, and are <2 to >20 μm along the maximum dimension. They occur only in the La Casita Formation.

Following the guidelines of Goldstein and Reynolds (1994), we identified fluid inclusion assemblages (FIAs) comprising groups of inclusions that formed at the same time. We discriminated primary FIAs as groups of inclusions that exhibited similar compositions and liquid:vapor ratios, and that were confined to a single growth zone in the host crystal (Figs. 7a, 8). Groups of inclusions comprising pseudosecondary FIAs likewise exhibited similar composition and liquid:vapor ratios, but were distributed in planar groups that did not cross all growth zones of the host crystal (Fig. 9). If such a planar array extended to a grain boundary, the FIA was classified as secondary (Goldstein and Reynolds, 1994). In circumstances where the origin of an FIA could not be confidently interpreted, it was classified as unknown.

4.1. Microthermometric methods

Conventional heating and freezing microthermometric analyses were performed on 94 vein samples, 69 of which were found to contain usable data. The analyses were conducted with a modified U.S. Geological Survey-type heating–freezing stage manufactured by FLUID Inc., and calibrated at 0 °C (ice bath), 374.1 °C (critical point of water), and −56.6 °C (CO_2 triple point) (the latter two standards supplied by SYNFLINC, Inc.). Samples were cut into doubly polished, 50–150 μm thick sections (e.g., Holland et al., 1978) and examined for the presence of suitably large (>2 μm) fluid inclusions. We kept the samples below 50 °C during preparation to avoid stretching or decrepitating any low temperature inclusions that might be present. To test whether our preparation process modified inclusions, results for inclusions in cleavage flakes were compared with those from polished thick sections of the same sample. Inclusion homogenization temperatures in thick sections and flakes were identical in every instance where we made such a comparison.

Fluid inclusion maps (Touret, 2001) were made of all inclusions in the field of view during a heating–cooling run. By recording the phase change temperatures of each inclusion on the map, systematic variations could be identified and used to recognize multiple fluid inclusion populations that might be present in a given field of view. Except as noted below, heating runs were conducted before freezing runs to reduce the possibility of inclusion stretching by freezing (Lawler and Crawford, 1983; Meunier, 1989). To limit the possibility of measuring inclusions that underwent post-entrapment leakage or stretching, we only measured FIAs in the same field of view during a single heating or freezing run. Individual inclusions that had no nearby inclusions within the same field of view were not measured. By restricting measurements to inclusion assemblages within the same field of view, any sudden changes in liquid:vapor ratios due to inclusion deformation could be observed, and the suspect inclusions were removed from consideration.

The two- and three-phase inclusions were heated and the homogenization temperature (T_h) was measured. Fluid inclusions with lower T_h were analyzed before those with a higher T_h to avoid overheating the fluid inclusions. All of the two-phase aqueous inclusions homogenized to a liquid. After heating, the two-phase inclusions were cooled to approximately −170 °C and slowly warmed to first observe the eutectic melting temperature (T_e), and then the final ice melting temperature (T_m). The dissolution temperature of the halite cube was recorded during heating of the three-phase inclusions. Halite dissolution occurred either before or after the homogenization of the vapor bubble. Ice melting temperatures were reproducible within 0.5 °C, whereas halite dissolution and homogenization values were reproducible within 2 °C. The composition of fluids in the two-phase aqueous inclusions was determined from standard phase diagrams of the NaCl–H_2O system (Crawford, 1981; Shepherd et al., 1985).

Although we attempted to obtain fluid inclusion measurements from all mineral stages in all vein types, we were limited by the quality of the mineralization, size of the inclusions, and inclusion deformation on heating. In general, quartz was relatively easy to work with and provided reliable, reproducible data. Calcite was difficult to work with because the fluid inclusions are generally less than 5 μm in size and the earliest stages of calcite are often moderately to extensively twined. Later stages of calcite were less deformed, however, and reliable and repeatable data were more readily obtained. In samples containing easily stretched or decrepitated inclusions, freezing, instead of heating, was done on several inclusions in order to obtain salinity data. Twelve such samples are included in our data set.

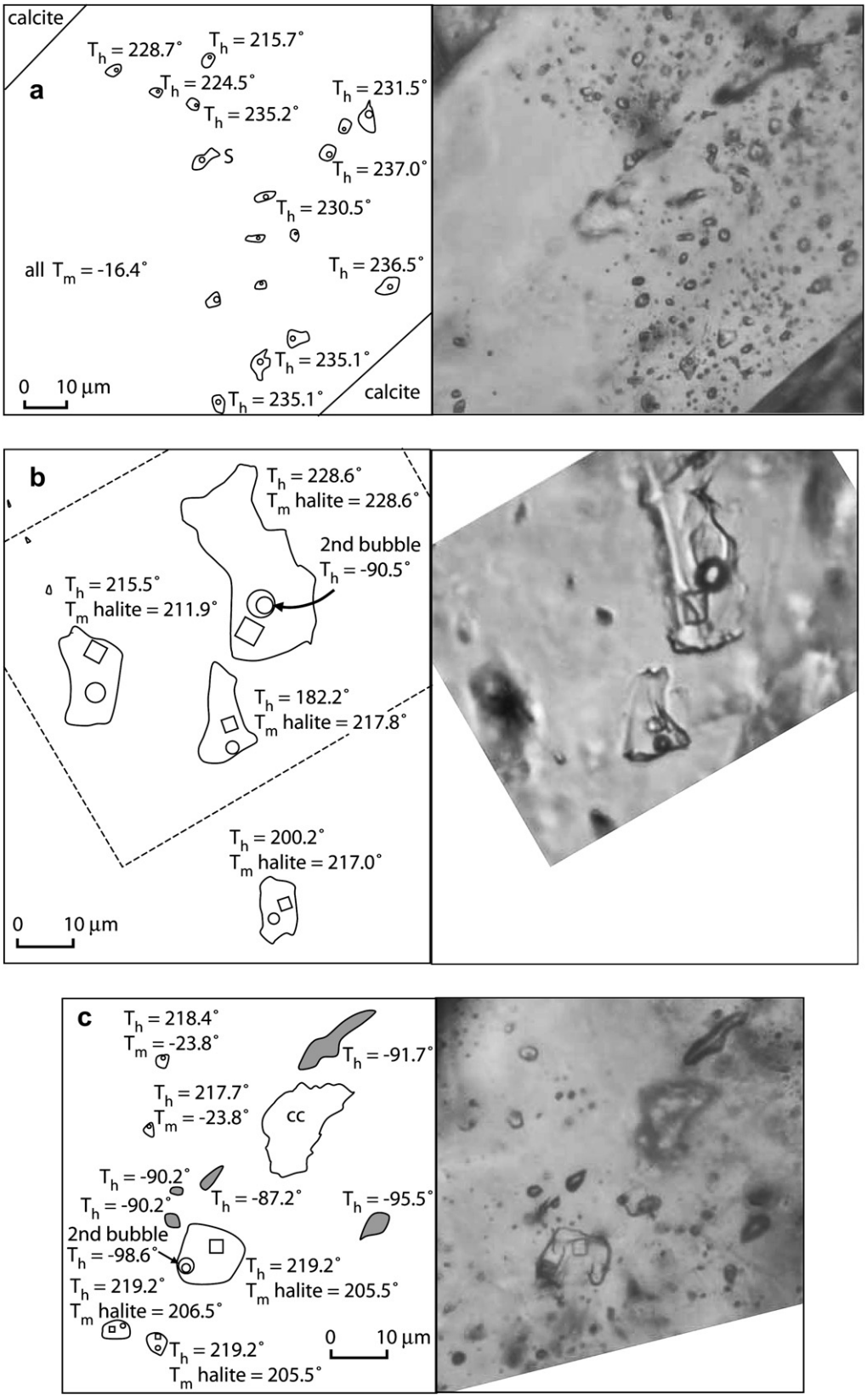

Fig. 7. Photomicrographs showing examples of the three types of inclusions we encountered in samples from the study area. (a) A primary assemblage of two-phase aqueous inclusions. (b) A primary assemblage of three-phase inclusions, one of which contains a double bubble. (c) A primary assemblage of single-phase inclusions. Note the presence of three-phase inclusions in the same field of view. All photos were taken at 25 °C and all examples are hosted in quartz from sample C012-LC4 in the La Casita Formation.

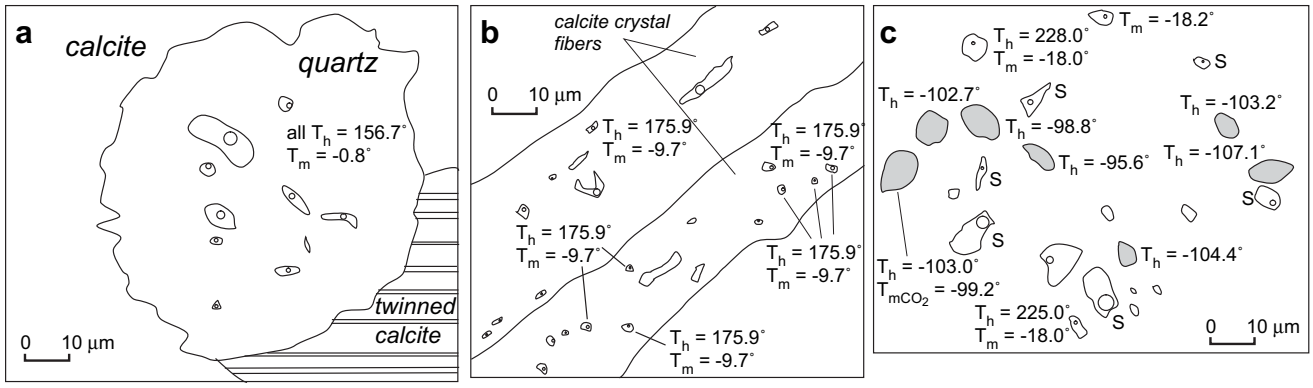

Fig. 8. (a) Primary inclusions in quartz that is surrounded by calcite in sample C165-2 from the Difunta Group. (b) Primary inclusions growing along the long axis of a calcite fiber in sample C010-LC6 from the La Casita Formation. (c) An assemblage of primary, coeval single- and two-phase inclusions from sample C012-LC4 in the La Casita Formation. The "S" in some figures denotes inclusions that stretched upon heating.

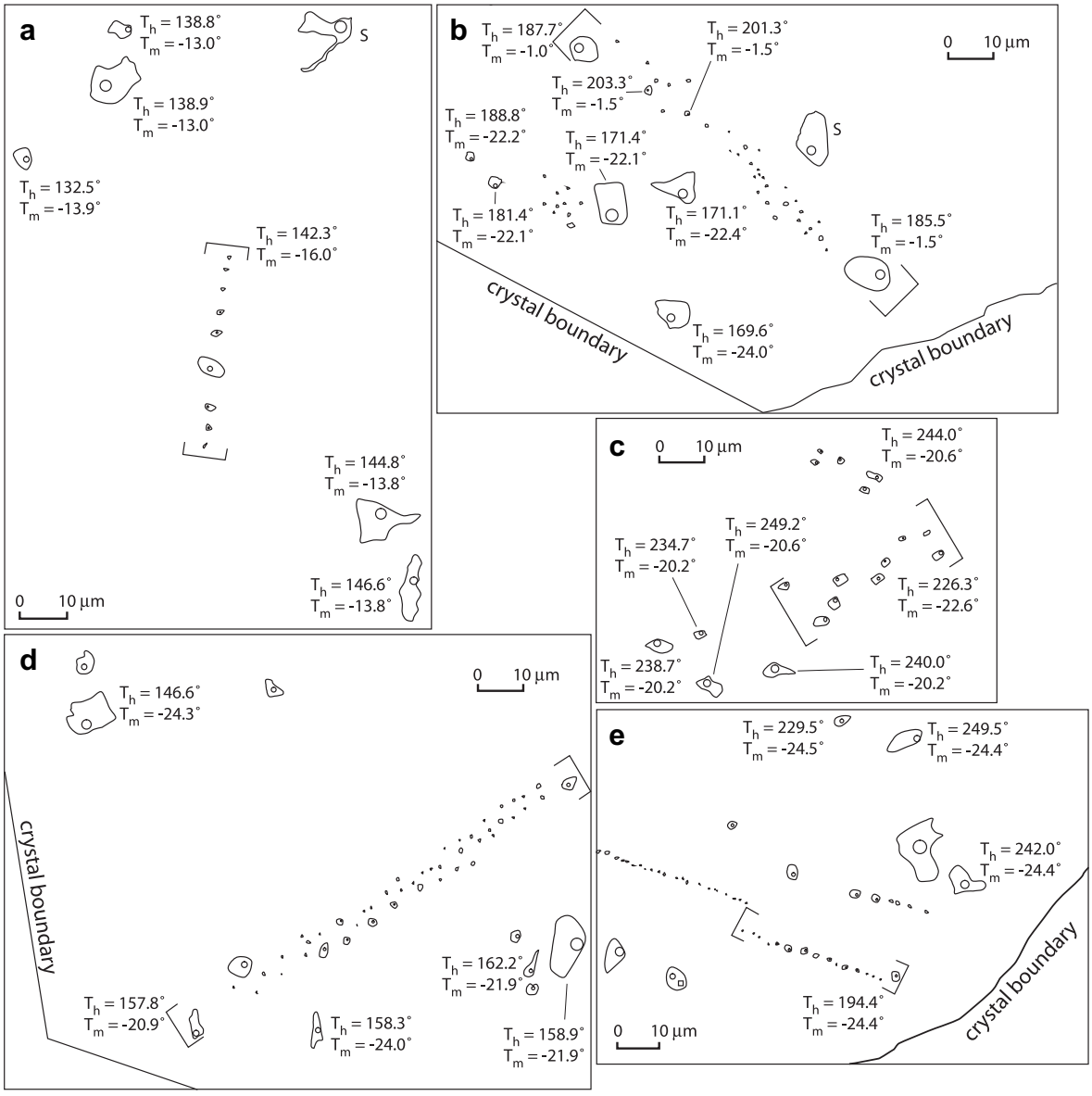

Fig. 9. Examples of pseudosecondary, aqueous fluid inclusion assemblages observed in samples from the study area. Pseudosecondary inclusions are highlighted by brackets. Other primary or secondary inclusions are also shown on (a) Inclusions in quartz of a stage 1 vein (sample C004-T2) from the Taraises Formation. (b) Inclusions in quartz of a stage 3 vein (sample C011-LC2) from the La Casita Formation. (c) Inclusions in quartz of a stage 1 vein (sample 9-v2) from the La Casita Formation. (d) Inclusions in calcite of a stage 1 vein (sample T-42B) from the Taraises Formation. (e) Inclusions in quartz of a stage 3 vein (C013-LC3) from the La Casita Formation. As in Fig. 8, the "S" in some figures denotes inclusions that stretched upon heating.

4.2. On methane in the regional fluid system

A variety of observations suggest that the aqueous fluids in our inclusions are methane saturated and were at their bubble point at the time of trapping. Upon crushing in kerosene, many of the two-phase aqueous inclusions and all of the tested single-phase inclusions released a bubble that formed immediately and completely dissolved in the surrounding kerosene, indicating the presence of CH_4 and/or soluble hydrocarbons (Roedder, 1973). Upon cooling to −170 °C, larger three-phase inclusions exhibited the formation of a vapor bubble within the original bubble. When heated, this second bubble homogenized into the liquid between −98.5 and −90.5 °C, indicating the presence of methane (Fig. 7b, c). The widespread occurrence of methane in the regional fluid system is further supported by the fact that single-phase methane inclusions occur in primary assemblages with two- and three-phase aqueous inclusions in several samples (Figs. 7c and 8c). This relationship requires that the methane inclusions were either trapped simultaneously with the aqueous inclusions, or at least trapped during the same mineral growth phase. In such a situation it is ordinarily interpreted that the aqueous inclusions were methane saturated at the time of trapping. We broadly make this same interpretation for all of the aqueous inclusions in this study.

4.2.1. Constraints on fluid trapping conditions

As noted by Mullis (1987), simultaneously trapped or genetically related aqueous and methane-rich inclusions can be used as a geothermometer and a geobarometer. Since the solubility of methane in brine increases with increasing temperature and pressure (Haas, 1978; Hanor, 1980), the fluid temperature at the time of trapping is equal to the T_h of the aqueous inclusions because this is the temperature at which all of the CH_4 is resorbed into the brine. As long as aqueous inclusions are saturated with methane during trapping, the intersection of the methane isochore and the T_h of the coeval aqueous inclusions on a pressure–temperature diagram determines the fluid pressure at the time of trapping. Here we use the "T_h–isochore intersection method" of Mullis (1987) to constrain the fluid trapping pressures. The data were obtained from primary and pseudosecondary FIAs in a stage 2 fault and primary FIAs in a stage 3 cross-fold vein in the La Casita Formation.

When single-phase inclusions in the samples were cooled to approximately −170 °C, they were found to contain two phases, a liquid and vapor, or, in one sample, three phases, a liquid, a vapor, and a solid. The liquid and vapor are CH_4 (ideal critical temperature of $CH_4 = -82.4$ °C), and the solid is CO_2 (ideal triple point temperature = −56.6 °C). Upon warming, the solid melting (sublimation) temperature (T_{mC}) and total homogenization temperature of the hydrocarbon inclusions (T_{hH}) were determined. Homogenization values in our two samples range from −85.6 °C to −107.1 °C, and the molar volume data for the system CO_2–CH_4 (van den Kerkhof, 1988, 1990; Kisch and van den Kerkhof, 1991), together with the measured T_{mC} of the solid CO_2, indicate that the three-phase inclusions contain approximately 5% CO_2.

Fig. 10 uses the aforementioned characteristics of the coeval aqueous and hydrocarbon inclusions to constrain the temperature and pressure conditions at the time the inclusions were trapped. In the stage 3 cross-fold vein where homogenization temperatures (T_h) for the aqueous inclusions range from 200° to 230 °C, the isochores for the coeval hydrocarbon inclusions constrain the trapping pressures to 120–175 MPa. These conditions are compatible with the stage 2 fault, which has aqueous inclusion T_h values between 215 and 237 °C and corresponding trapping pressures of 138–148 MPa. In contrast to these similar values in two different samples, the isochore for a pseudosecondary FIA in the same stage 3 cross-fold vein constrains the trapping pressures to lie between 55 and 60 MPa. Assuming a geothermal gradient between 30 and 40 °C, the primary FIAs in the stage 2 and stage 3 veins appear to have formed at near lithostatic pressures, whereas the pseudosecondary FIAs in the stage 3 vein are best interpreted as forming at nearly hydrostatic pressures (Fig. 10). The coexistence of high and low pressure FIAs in sample C012-LC4 suggests there may have been significant fluid pressure variations during formation of cross-fold veins. These fluid pressure variations suggest the veins were reopened and reactivated at depths that were up to 3 km different.

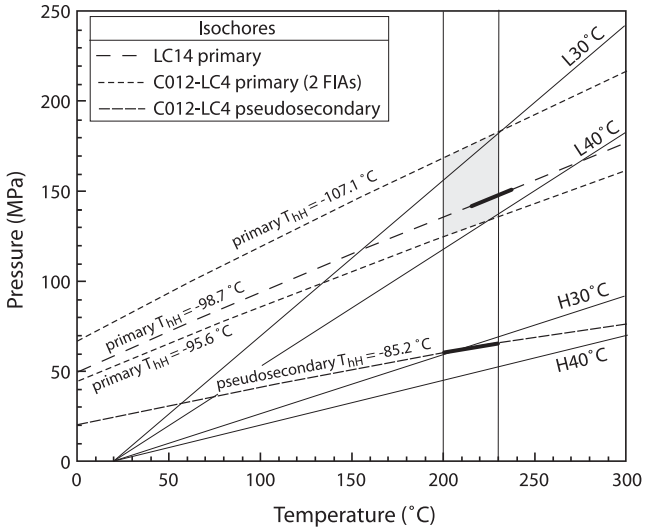

Fig. 10. Temperature and pressure conditions during trapping of coeval hydrocarbon and aqueous inclusions in stage 2 vein sample LC14 and stage 3 vein sample C012-LC4 of the La Casita Formation. Isochores for the H_2O–CO_2–CH_4 system were determined from the equations of state presented in Duan et al. (1992a,b). Four different pressure–temperature relations are shown for reference; H30 °C and H40 °C respectively assume hydrostatic stress and geothermal gradients of 30 °C km^{-1} and 40 °C km^{-1}, whereas L30 °C and L40 °C assume the same geothermal gradients and lithostatic stress. Pressure gradients are assumed to be 26 MPa km^{-1} for the lithostats, and 10 MPa km^{-1} for the hydrostats. A paleosurface temperature of 20 °C is also assumed. The upper shaded area constrains the pressure–temperature conditions under which the primary inclusions formed in the stage 3 vein sample. The upper heavy line shows the conditions under which the primary inclusions formed in the stage 2 vein, whereas the lower heavy line shows the conditions under which the pseudosecondary inclusions formed in the stage 3 vein.

4.3. Characteristics of fluid inclusions in each stratigraphic unit

Here we summarize the homogenization temperatures, salinities and estimated brine compositions of the aqueous fluid inclusion assemblages we analyzed. Because we are interested in the regional paleohydrologic system that operated on the scale of hundreds to thousands of meters, we emphasize the broad similarities amongst samples and de-emphasize the fine-scale variations within individual samples. In so doing, we assert that broad similarities constrain the large-scale, long-lived characteristics of the paleohydrologic system, whereas fine-scale variations within individual samples may constrain only the specific, short-term paleohydrology of one part of one vein. Although it is likely that fluids of differing composition were stratigraphically segregated at scales smaller than that of individual formations, we cannot resolve these differences. We group our observed fluid types at the formation scale for convenience only.

Fluid inclusion assemblages in samples from the Difunta Group are strikingly similar, irrespective of their host mineral, origin, or vein stage. As shown in Fig. 11a, all but two assemblages have salinities less than 4 wt% NaCl equivalent, and the majority of assemblages exhibit T_h values between 125 and 178 °C. One primary

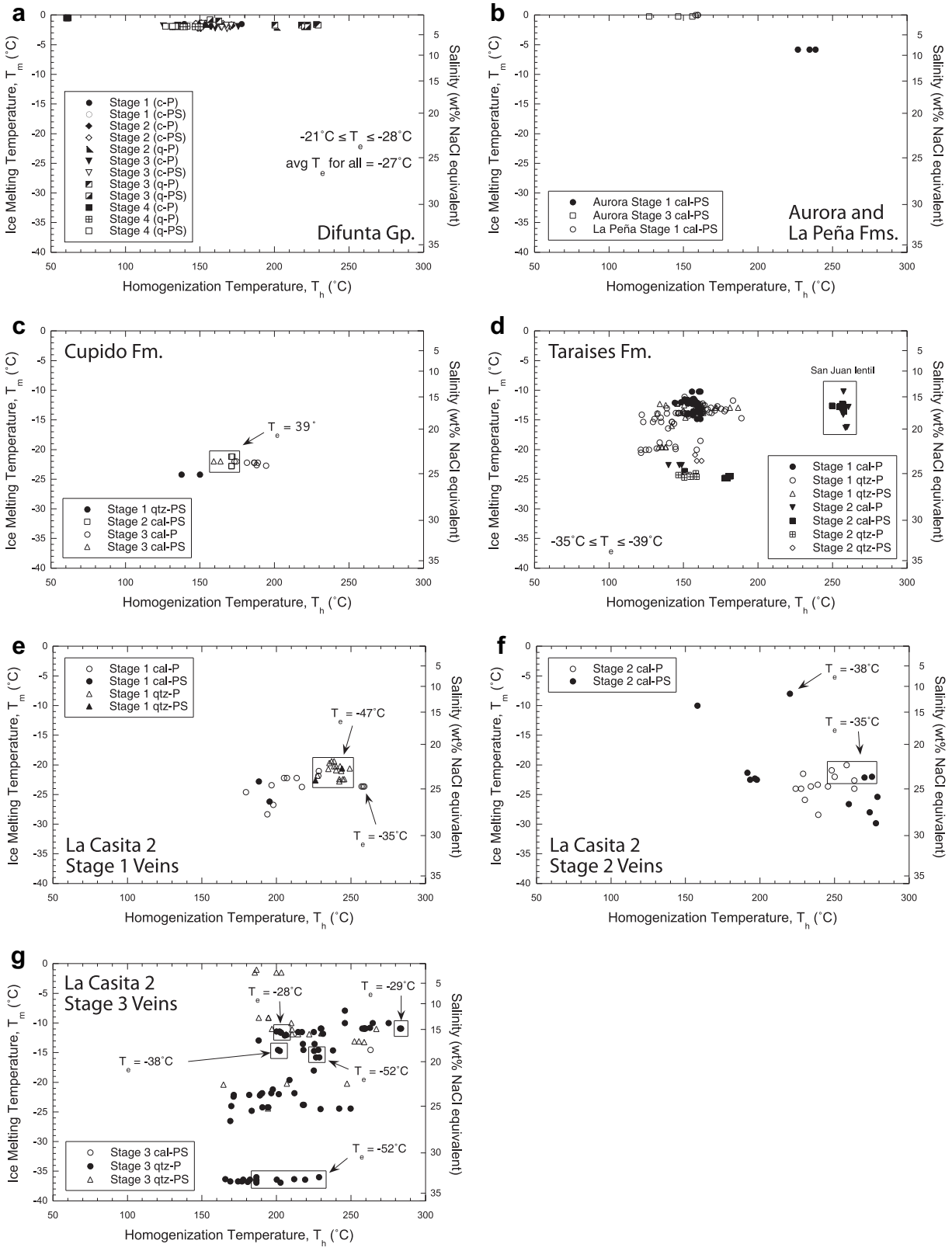

Fig. 11. Summary graphs of homogenization temperature (T_h) versus ice melting temperature (T_m) and salinity for various rock units exposed in the study area. In all the plots, stages 1–4 refer to the various vein stages defined by field and petrographic criteria, cal and qtz respectively refer to inclusions that are hosted in calcite or quartz, and P and PS respectively refer to FIAs interpreted as primary or pseudosecondary. (a) Data from the Difunta Group. (b) Data from the Aurora and La Peña Formations. (c) Data from the Cupido Formation. (d) Data from the Taraises Formation. (e) Data from stage 1 veins in the La Casita 2. (f) Data from stage 2 veins in the La Casita 2. (g) Data from stage 3 veins in the La Casita 2. See Fig. 3 for the regional stratigraphic column.

assemblage from early calcite in a stage 4 vein shows T_h values near 60 °C, whereas primary and pseudosecondary assemblages in late quartz in a stage 3 vein exhibit T_h values between 200 and 230 °C. Eutectic melting temperatures (T_e) in inclusions from the Difunta Group are always near 28 °C, indicating a brine composition in the NaCl–H_2O system.

We obtained reliable data from a total of only three samples in the Aurora and La Peña Formations. Although we could not obtain eutectic melting temperatures for any of these assemblages, Fig. 11b shows that two of the three assemblages we analyzed have near zero salinities and T_h values between 127 and 160 °C. The third assemblage was from later, untwined calcite in a stage 1 vein, and yielded T_h values near 230 °C and salinities near 9 wt% NaCl equivalent.

Despite extensive sampling in the Cupido Formation, only three veins contained FIAs that yielded reliable, reproducible data. These data were obtained primarily from later, less twined or clear calcite, as inclusions in earlier, more extensively twined calcite were prone to decrepitation. As shown in Fig. 11c the data do not vary significantly with inclusion origin or host mineral, with T_h values ranging from 137 to 195 °C and salinities averaging near 24 wt% NaCl equivalent. Eutectic melting temperatures obtained from two assemblages are near −39 °C, indicating a brine composition of $NaCl \pm CaCl_2 \pm MgCl_2 \pm H_2O$.

Although veins from stages 1 through 3 are developed in the Taraises Formation, we only obtained useable data from samples of vein stages 1 and 2. As shown in Fig. 11d the FIAs in these samples show three noteworthy characteristics. First, in the San Juan lentil, a roughly 40 m thick carbonate unit at the base of the Taraises Formation (Fig. 3), all FIAs from a stage 2 vein exhibit an average T_h of 256 °C and salinities near 17 wt% NaCl equivalent. These salinities are similar to other FIAs in the Taraises Formation, but the T_h values are nearly 100 °C greater than the typical T_h observed elsewhere in the formation. Second, with the exception of the San Juan lentil, there is a generally similar range of T_h and salinity for all FIAs in the Taraises Formation, irrespective of inclusion origin, host mineral or vein stage (Fig. 11d). Although it could be argued that the range of T_h is greater in quartz-hosted FIAs than in calcite-hosted FIAs, the overall average T_h is near 155 °C and the range of salinities is from 16 to 25 wt% NaCl equivalent. Third, the average eutectic melting temperatures lie between −35 and −39 °C in several FIAs from the shaley part of the Taraises Formation. Like the Cupido Formation, these results suggest the brine composition in this part of the unit comprised $NaCl \pm CaCl_2 \pm MgCl_2 \pm H_2O$.

Samples from the La Casita Formation proved to be the easiest to work with and we consequently obtained abundant, useful data from a variety of veins in various structural positions. As shown in Fig. 11e, f and g, FIAs in vein stages 1–3 in the La Casita 2 (Fig. 3) show little systematic variation according to inclusion origin or host mineral. Stage 1 veins in this upper part of the La Casita Formation exhibit salinities between 23 and 28 wt% NaCl equivalent, and T_h values from 180 to 260 °C, with the average near 230 °C (Fig. 11e). Eutectic melting temperatures of several FIAs in stage 1 veins are near −47 °C, with one FIA yielding a T_e of −35 °C. These values suggest a brine composition of $NaCl \pm CaCl_2 \pm MgCl_2 \pm H_2O$. In contrast, fluid inclusion assemblages from stage 2 and stage 3 veins in the La Casita 2 yield T_h values that range from 158 to 285 °C and salinities that vary from 2 to 29 wt% NaCl, with stage 3 veins exhibiting the greatest variation in both T_h and salinity (Fig. 11f, g). Assemblages in stage 2 veins yield T_e values from −35 to −38 °C whereas FIAs in stage 3 veins yield T_e values from −28 to −52 °C. The T_e data in the stage 3 veins show a weak, inverse relationship with inclusion salinity such that lower eutectic temperatures are often correlated with higher salinities.

Fig. 12a, b and c summarizes the characteristics of fluid inclusions in the lower part of the La Casita Formation, the La Casita 1 (Fig. 3). Here the T_e values also show a weak, inverse correlation with salinity, and range from −28 to −52 °C. There is no obvious systematic variation in FIA characteristics as a function of host

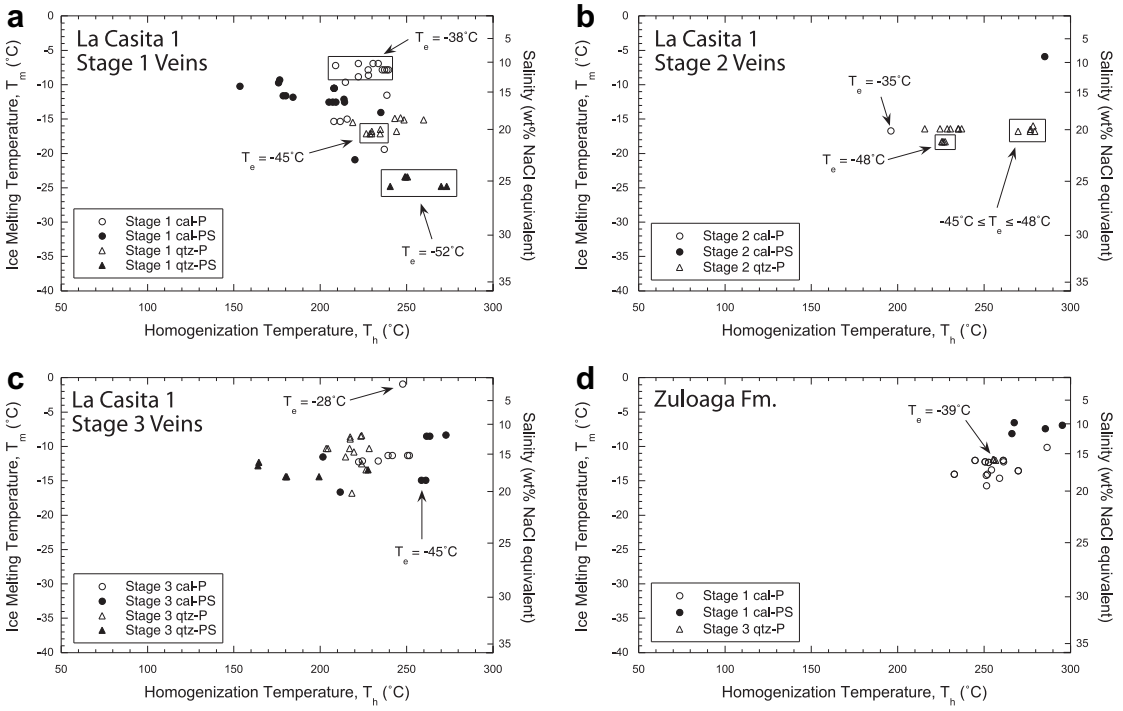

Fig. 12. Summary graphs of homogenization temperature (T_h) versus ice melting temperature (T_m) and salinity for various rock units exposed in the study area. In all the plots, stages 1–4 refer to the various vein stages defined by field and petrographic criteria, cal and qtz respectively refer to inclusions that are hosted in calcite or quartz, and P and PS respectively refer to FIAs interpreted as primary or pseudosecondary. (a) Data from the stage 1 veins in the La Casita 1. (b) Data from stage 2 veins in the La Casita 1. (c) Data from stage 3 veins in the La Casita 1. (d) Data from the Zuloaga Formation. See Fig. 3 for the regional stratigraphic column.

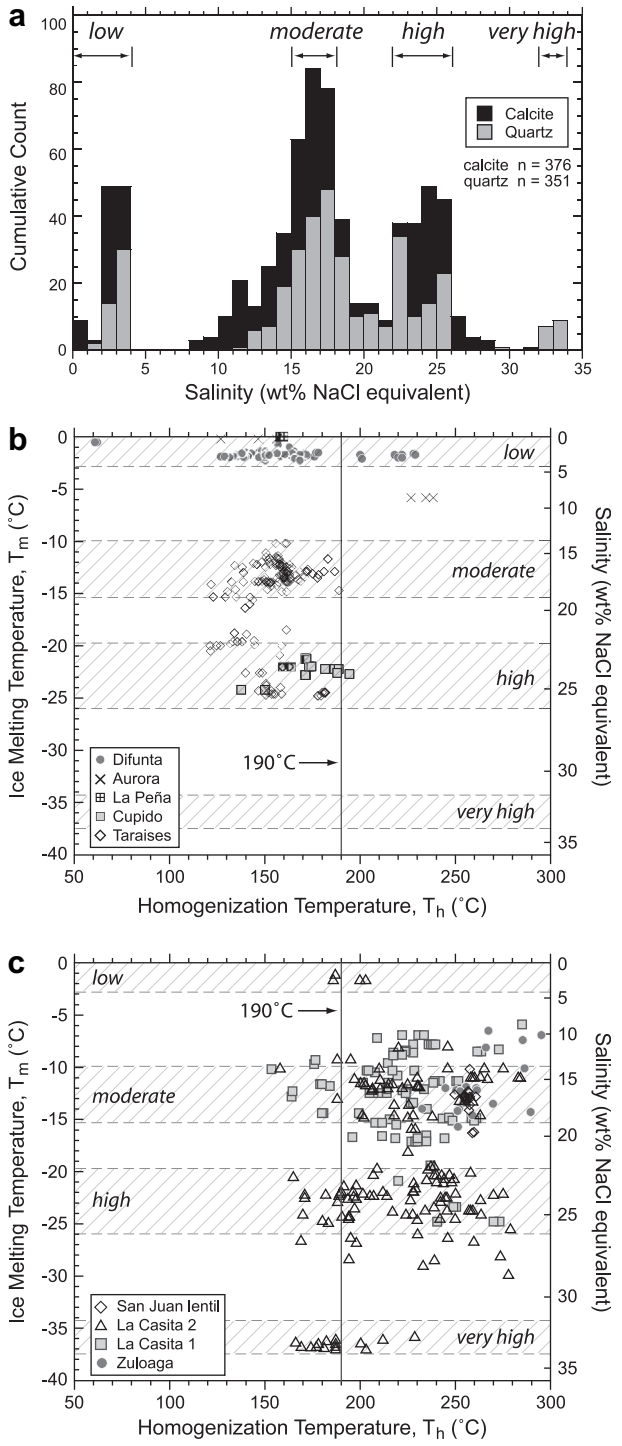

Fig. 13. Summary of fluid inclusion data for the Nuncios Fold Complex. Data are divided into the lower two graphs for visual clarity, and are not discriminated by vein stage, inclusion type or host mineral. Each data point represents one measured inclusion. (a) Histogram of fluid inclusion salinities in all samples. Salinities in two-phase aqueous inclusions are calculated from T_m using the equation of Bodnar (1992). Salinities in three-phase aqueous inclusions were calculated from the melting temperature of a halite cube (Sterner et al., 1988; Goldstein and Reynolds, 1994). Note that salinities do not correlate with host mineral. (b) Fluid inclusion homogenization temperatures and salinities for veins from the Difunta Group through the Taraises Formation, exclusive of the San Juan lentil. (c) Fluid inclusion homogenization temperatures and salinities for veins from the San Juan lentil through the Zuloaga Formation. Lined areas in (b) and (c) denote the four salinity groups identified in part (a). See Fig. 3 for the regional stratigraphic column.

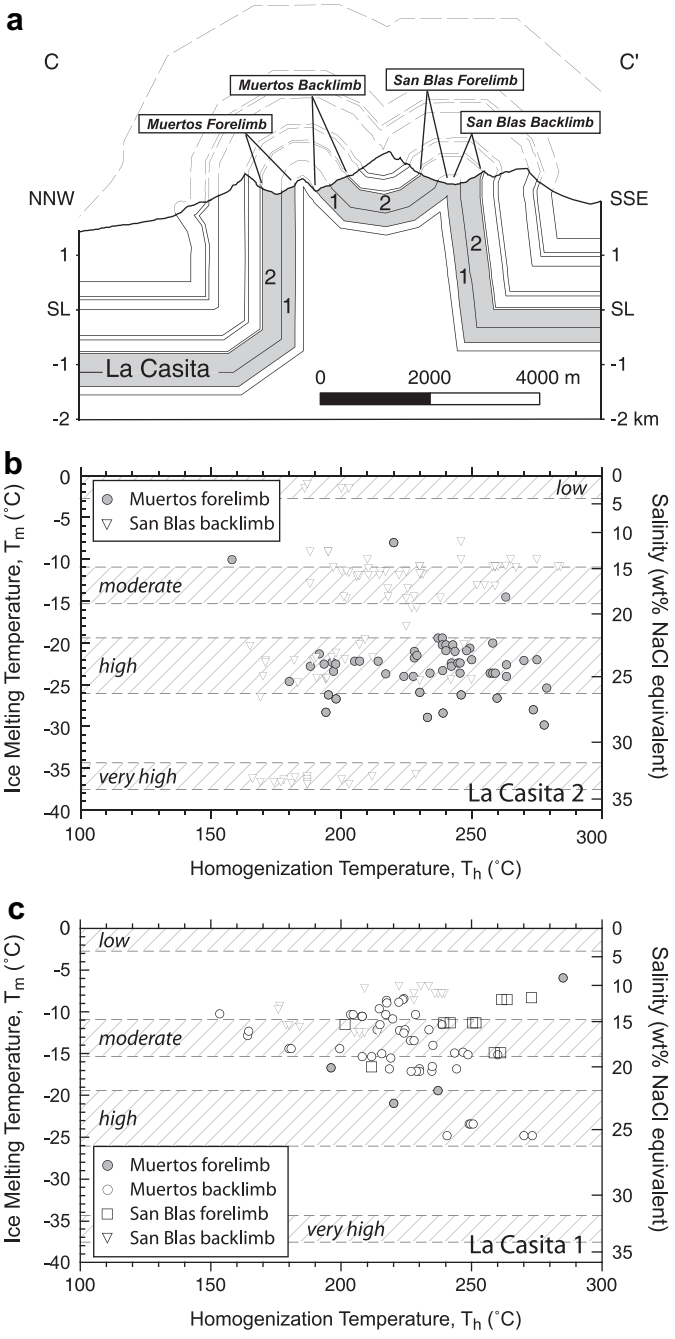

Fig. 14. Summary of fluid inclusion data in the La Casita Formation. (a) Geological cross section C–C′ through the Nuncios Fold Complex; four examined structural positions and the two informal subdivisions of the La Casita Formation are shown for reference. See Fig. 2 for section location. (b) Fluid inclusion homogenization temperatures and salinities in the La Casita 2, plotted according to structural position. (c) Fluid inclusion homogenization temperatures and salinities in the La Casita 1, plotted according to structural position. Data are not discriminated by vein stage, inclusion origin or host mineral. Each data point represents one measured inclusion in parts (b) and (c). Lined areas in (b) and (c) denote the four salinity groups identified in Fig. 13a.

mineral or inclusion origin, and similar to the overlying La Casita 2 unit, both salinity and T_h values vary over significant ranges. Assemblages in stage 1 veins show salinities that vary from 10 to 23 wt% NaCl equivalent and T_h values that range from 153 to 260 °C (Fig. 12a). Assemblages in stage 2 veins yield T_h values from 195 to 285 °C, and average salinities near 23 wt% NaCl equivalent (Fig. 12b). In stage 3 veins, FIAs yield T_h values ranging from 164 to 273 °C, and

salinities from 2 to 20 wt% NaCl (Fig. 12c). In stage 3 veins the T_h range is less in primary FIAs than in pseudosecondary FIAs.

In the Zuloaga Formation our FIA data come from only two samples, one from a stage 1 vein and one from a stage 3 vein. Both samples were taken from the core of the Muertos Anticline, the only location where the formation is exposed. Despite coming from very different veins and host minerals, primary assemblages in calcite in the stage 1 vein are similar to those in later quartz in the stage 3 vein (Fig. 12d). Homogenization temperatures in these assemblages cluster near 255 °C and salinities average near 18 wt% NaCl equivalent. A pseudosecondary assemblage in the stage 1 vein shows slightly higher T_h values of 267 °C to 295 °C and slightly lower salinity near 10 wt% NaCl equivalent. Eutectic melting temperatures in FIAs in both samples are −39 °C, indicating a brine composition of $NaCl \pm CaCl_2 \pm MgCl_2 \pm H_2O$.

4.4. Data synthesis: variables controlling the paleohydrologic system

A principal goal of our study was to determine whether the key variables of stratigraphy, structural position and progressive deformation affected the structure and evolution of the regional paleohydrologic system. We tested for such effects by searching the data for trends and patterns that might correlate with these variables. Despite our very high sampling density we do not have enough data to reliably search for these trends in each vein stage or in each stratigraphic unit or structural position in the area. Consequently, and because fewer than 15% of the samples yielded data that varied according to either inclusion origin or host mineral (Figs. 11 and 12), we ignore all these variables in the following analysis. In so doing, we recognize that we can only resolve the regional-scale characteristics of the paleohydrologic system.

4.4.1. Regional variation in fluids with stratigraphy

Fig. 13 demonstrates that irrespective of vein timing, position in the NFC, inclusion origin or host mineral, fluids in the region can be divided into four distinct salinity classes and two broad T_h ranges. Salinities can be divided into low (0–5 wt% NaCl equiv.), moderate (15–18 wt% NaCl equiv.), high (22–26 wt% NaCl equiv.), or very high (32–34 wt% NaCl equiv.) groups (Fig. 13a). Although the overall range of T_h is large throughout the entire stratigraphic column, a distinct break occurs at the top of the San Juan lentil at the base of the Taraises Formation. Above this boundary the data are generally more tightly clustered, T_h values are almost entirely below 190 °C,

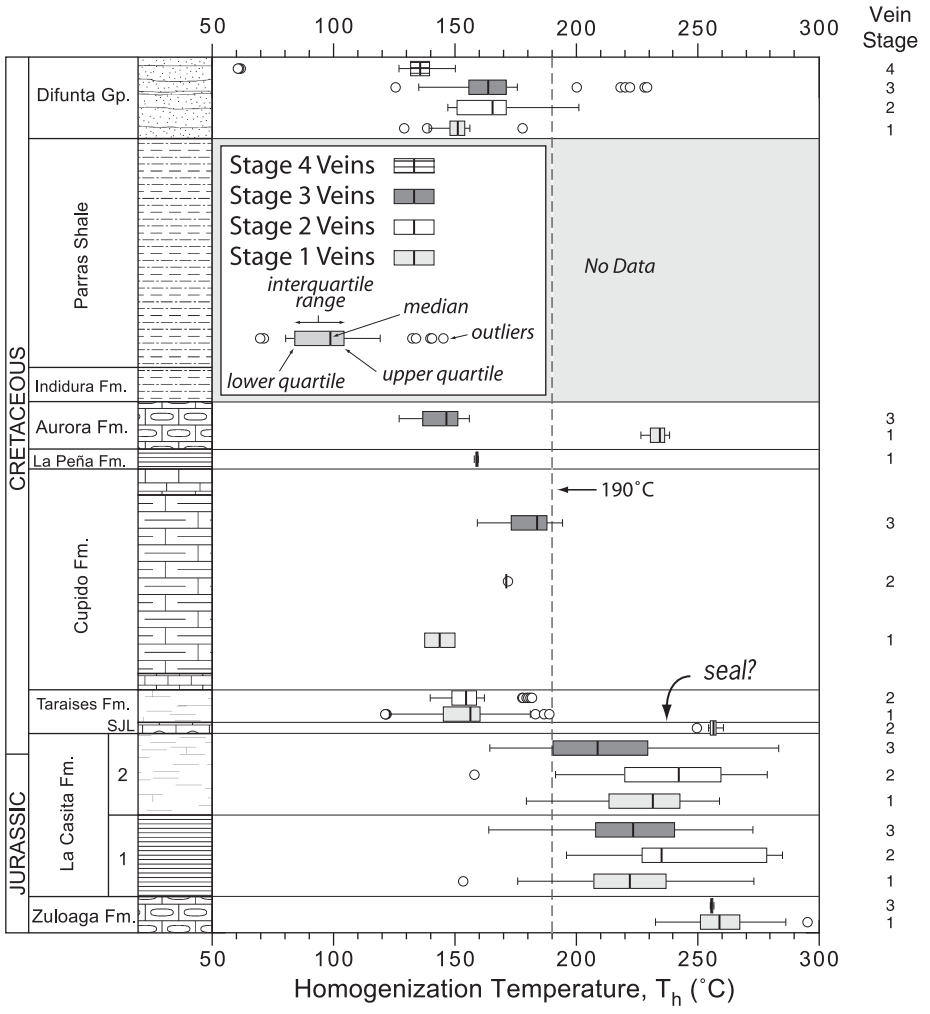

Fig. 15. Homogenization temperatures for fluid inclusions as a function of vein stage and stratigraphy. Box plots show the median, upper quartile (UQ), lower quartile (LQ), interquartile range (IR = UQ − LQ), and outliers of all T_h values measured in all fluid inclusion assemblages for a given vein stage in each stratigraphic unit. The ends of the whiskers on each box show the values of the largest and smallest data points whose values are either >UQ + 1.5 * IR or <LQ − 1.5 * IR. Any data points that lie outside of the whiskers are considered outliers and are plotted as individual points. The vein stage represented by each box plot is listed in the column on the right side of the graph. Note that although the vertical dimension of the plot is scaled to accurately reflect the relative stratigraphic thickness of each labeled unit, the vertical position of each box plot is not intended to represent the specific location of a given stage of veins in a given stratigraphic unit; they are simply drawn so that vein stages increase upward in each unit.

and the average value is near 150 °C (Fig. 13b). Salinities in this part of the section are low, moderate or high, and no veins contain very high salinity fluids. Below the top of the San Juan lentil the data are more scattered, T_h values are primarily above 190 °C, and average near 225 °C (Fig. 13c). Moderate and high salinity fluids dominate this part of the stratigraphic section, with low salinity fluids observed in only one stage 3 vein in the La Casita 2, and very high salinity fluids observed in several veins.

Though less well constrained than the boundary at the San Juan lentil, a second fluid boundary is suggested by the concentration of low salinity fluids in veins of the Difunta Group (Fig. 13b). Veins in nearly every other unit contain FIAs with salinities from at least one of the other salinity groups (Fig. 13a), and with the exception of our one sample from the La Peña Formation, all contain fluids with salinities that are greater than 10 wt% NaCl equivalent. Unfortunately the general scarcity of veins and lack of exposure of rocks from the Indidura Formation and Parras Shale make it difficult to precisely locate the stratigraphic position of this boundary and although our limited data from the Aurora and La Peña Formations suggest it may be as low as the top of the Cupido Formation, this is equivocal. Moreover, because Difunta Group rocks are not preserved over the NFC, it is unclear whether this was a stratigraphic control on the paleohydrologic system, or whether it represents a basin-scale structural partitioning of fluids between the Sierra Madre Oriental fold belt and the adjacent Parras Basin (Figs. 1 and 2).

4.4.2. Regional variation in fluids with structural position

To test whether fluids were partitioned by structural position within the NFC we compared fluids in the La Casita Formation where it is exposed in four structural positions defined by the limbs of the Muertos and San Blas anticlines. We chose this unit because it was the only one from which we had multiple samples from each vein stage in each structural position. As shown in Fig. 14, fluids in the La Casita Formation show different degrees of structural partitioning as a function of stratigraphic position. Although the T_h of fluids is independent of structural position in the La Casita 2, the salinity data in this unit suggest that there was some degree of structural partitioning (Fig. 13b). Fluids from all four salinity groups are present in the backlimb of San Blas anticline, along the southern side of the fold complex. On the northern side of the structure, the forelimb of Muertos anticline almost exclusively contains high salinity fluids (22–26 wt% NaCl equiv.). By comparison, veins in the La Casita 1 show no evidence of partitioning according to structural position. Irrespective of relative timing, veins in this shale-dominated part of the section contain inclusions with a variety of T_h values and salinities that span the moderate and high ranges (Fig. 13c).

4.4.3. Regional variation in fluids with progressive deformation

To test whether fluid temperature or salinity varied systematically during folding, we separated the data by vein stage in each lithostratigraphic unit and searched for trends. Because our different

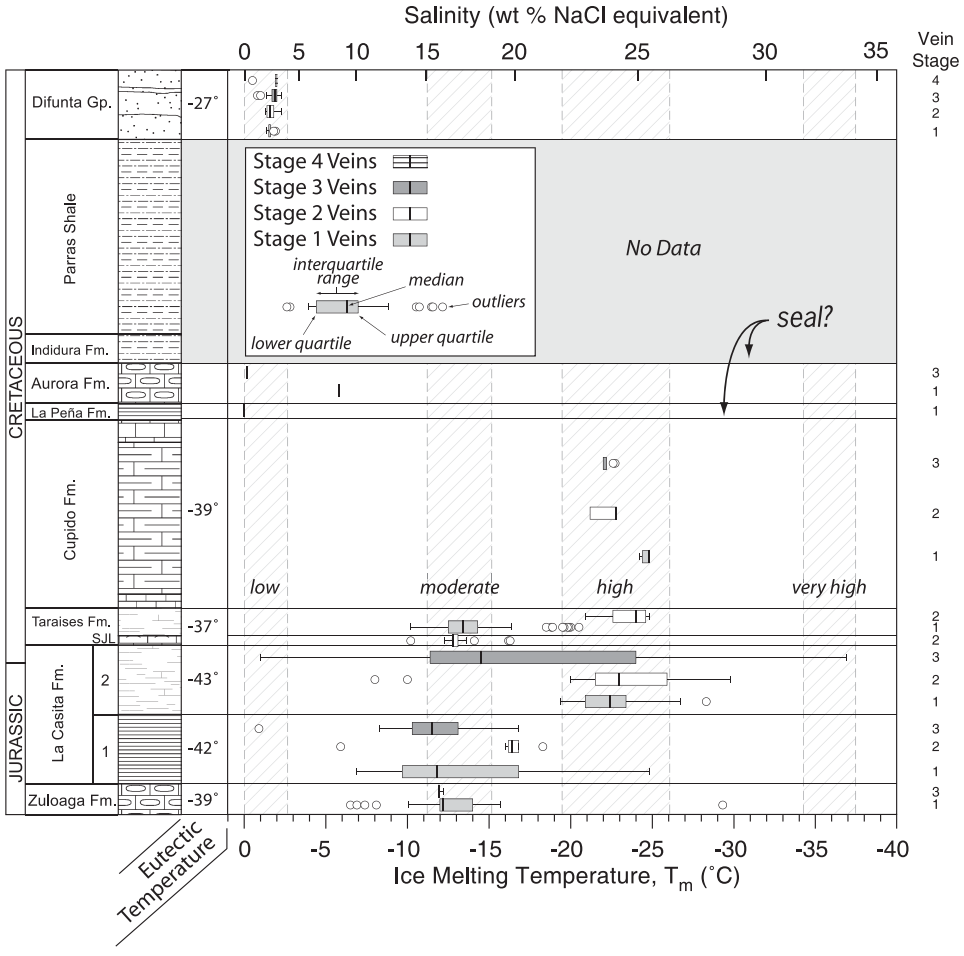

Fig. 16. Ice melting temperatures and salinities for fluid inclusions as a function of vein stage and stratigraphy. The four vertical lined areas correspond to the four salinity groups identified in Fig. 13a. Eutectic temperatures (T_e) are reported in degrees Celsius, and are the averages of all the measurements for all vein stages in each stratigraphic unit. Note that although the vertical dimension of the plot is scaled to accurately reflect the relative stratigraphic thickness of each labeled unit, the vertical position of each box plot is not intended to represent the specific location of a given stage of veins in a given stratigraphic unit; they are simply drawn so that vein stages increase upward in each unit. The specific vein stage represented by each box plot is listed in the column on the right side of the graph. The general characteristics of box plots are explained in Fig. 15.

vein stages formed during sequential phases of the progressive folding process, temporal variations in regional fluids should be indicated by trends in the data whenever T_h or salinity are plotted against vein stage. Fig. 15 reveals that inclusion T_h does not vary with the stages of vein formation we interpret for the NFC. Although T_h is significantly different across the top of the San Juan lentil, fluids above this seal are generally near 150 °C during every stage of vein formation. Fluids within and below the San Juan lentil are generally between 200 and 250 °C, but there is likewise no systematic variation in T_h with vein stage in this part of the section. Fig. 16 shows that fluid salinities, like T_h, also do not vary with vein stage. In veins from the Cupido and older formations, inclusion salinities are mostly in the moderate and high categories. In veins from rocks that are younger than the Cupido Fm. inclusion salinities are almost exclusively in the range of meteoric waters. As with the deeper part of the section, there is no variation in fluid salinity with vein stage.

5. Discussion

The paleohydrologic record we observe today in the Nuncios Fold Complex is a combination of two things: (1) the original hydrologic system that existed prior to the onset of folding, and (2) a fracture-modified hydrologic system that developed during folding and uplift. Although the characteristics of the original hydrologic system are unknown, it is likely to have been similar to other systems in lightly deformed sedimentary rocks and almost certainly included fractures (e.g., Laubach, 1988; Gale and Gomez, 2007). For at least 75 million years prior to the onset of folding in the Late Cretaceous, northeastern Mexico was alternately a foreland basin or a passive margin basin with an extensive carbonate bank (Wilson et al., 1984). As shown in Fig. 17, we suggest that there are two end-member types of hydrologic systems that can develop in similar areas comprised of thick sequences of subhorizontal, lightly deformed, siliciclastic and carbonate rock. Vertically connected hydrologic systems occur when aquifers at different depths can readily exchange fluids. Fluid composition (e.g., salinity) in these systems may be similar throughout the stratigraphic section, or it may vary gradually and systematically with depth (Fig. 17a). Fluid temperature in a vertically connected system is most likely controlled by burial depth because efficient vertical mixing will rapidly distribute any local influx of hydrothermal fluids (Fig. 17b). As shown in Fig. 17c and d, vertically stratified systems occur where aquifers at different depths are not hydrologically connected. Reservoirs in these systems will most likely contain unique fluids whose composition may be related to that of the host rock, and whose temperature is related to burial depth (Fig. 17c, d). Anomalous, irregular or locally inverted temperature profiles might be caused by the production or influx of hydrothermal fluids or hydrocarbon generation at a given stratigraphic level.

We hypothesize that fold-related fracturing like that in the Nuncios Fold Complex would primarily modify the connectivity of the pre-folding hydrologic system. These modifications will be largely unrecognizable in a vertically connected system because such a system already contains efficient pathways for fluid migration. In contrast, fold-related fracturing will noticeably increase the transmissivity of fluids in a vertically stratified hydrologic system, potentially destroying reservoir compartments and stratigraphic seals. In such a situation, the nature of fluid communication and the preservation of migrating fluids in vein fills will primarily depend on fluid advection and fracture sealing rates, although the volume of migrating fluid, pressure differences across sealing layers and fluid mixing rates may also play a role (Fig. 18).

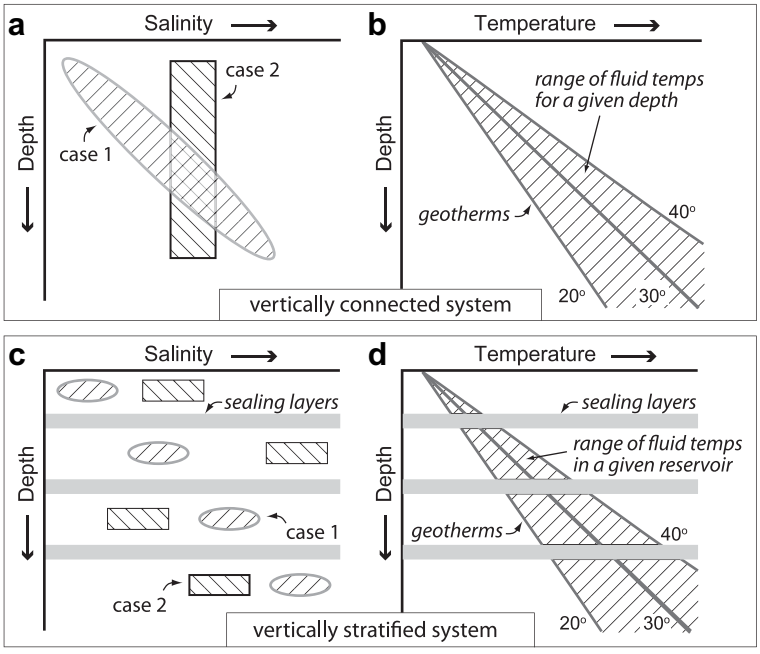

Fig. 17. Simplified models of hydrologic systems in lightly deformed, subhorizontal sedimentary rocks. Salinity is shown as an example characteristic of fluid composition. (a) and (b) represent a vertically connected system. The oval area on the salinity graph in (a) describes a case where shallow meteoric fluids gradually give way to highly saline brines at depth. The rectangular area in (a) describes a case where fluids are well mixed and salinities are similar throughout the entire stratigraphic section. The lined area on the temperature graph in (b) shows that fluid temperatures will gradually increase with depth according to the local geothermal gradient. (c) and (d) represent a vertically stratified system where persistent seals separate fluid reservoirs. Oval areas on the salinity graph in (c) describe a case where fluids are unique in each reservoir and salinity increases systematically with depth. Rectangular areas in (c) describe a case where fluids are unique in each reservoir and salinity varies non-systematically with depth. The temperature graph in (d) shows that temperatures will gradually increase with depth according to the local geothermal gradient, although processes such as hydrocarbon maturation or the influx of hydrothermal fluids may cause stratigraphically confined temperature anomalies. Although the reservoirs and seals in (c) and (d) are likely to occur at specific lithostratigraphic positions, their boundaries are not necessarily coincident with members, formations, groups or other formal stratigraphic units. The diagram here is entirely schematic and should not be interpreted to imply anything specific about thicknesses or positions of reservoirs and seals.

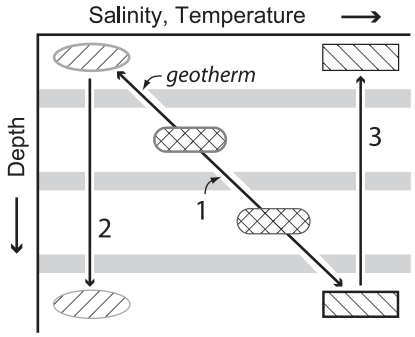

Fig. 18. Types of fluid communication that might occur in response to fracturing in a vertically stratified hydrologic system. Schematic graph shows pathways by which fluids of differing salinity and temperature in one reservoir can migrate into a different reservoir. Path 1 represents a mixing trend between shallow and deep fluids and will result in fluids whose salinity and temperature are intermediate between that of the communicating reservoirs. Slower advection and slower fracture sealing favor this path. Path 2 represents downward migrating meteoric water that does not mix with local fluids and will result in anomalously cool or low salinity fluids in deeper parts of the section. Path 3 represents upward migrating brine that does not mix with local fluids and will result in anomalously hot or high salinity fluids in the shallower parts of the section. Paths 2 and 3 are favored by faster advection and faster fracture sealing. Faster fluid mixing, slower advection, and slower fracture sealing will cause a shift from paths 2 and 3 toward path 1.

The competition between fracture formation, sealing and reactivation is particularly important because it may cause fractured aquifers in a detachment fold to become increasingly better connected, or only periodically connected. The former case occurs when sealing is always slow compared to fracture formation and reactivation; the latter case occurs when sealing is relatively rapid. In the case of rapid sealing, progressive, spatio-temporal variations in fracturing and mineralization will cause the system to intermittently become connected and then sealed, then reconnected, and then resealed, etc. This behavior should lead to a spatially varying vein record wherein some veins preserve multiple, distinct fluid types, whereas other veins do not. In contrast, wholesale, progressive increases in connectivity should generally transform a vertically stratified hydrologic system into a vertically connected one. Regardless of stratigraphic or structural position, veins in this system should consequently preserve fluids that are generally homogeneous, or that systematically vary with depth (e.g., Fig. 17a, b).

The paleohydrologic system of the Nuncios Fold Complex is best interpreted as a vertically stratified system that was periodically and repeatedly connected by fold-related fracturing (Fig. 19a). The stratified nature of the system is suggested by the large-scale, stratigraphic compartmentalization of fluids of certain salinities or temperatures (Figs. 15 and 16). An upper paleohydrostratigraphic unit was dominated by meteoric fluids that circulated deeply enough to be warmed to temperatures near 150 °C in rocks of the Difunta Group through Indidura Formation (Figs. 13b and 19a). Moderate to high salinity fluids near 150 °C dominated a middle paleohydrostratigraphic unit comprising the Cupido and Taraises

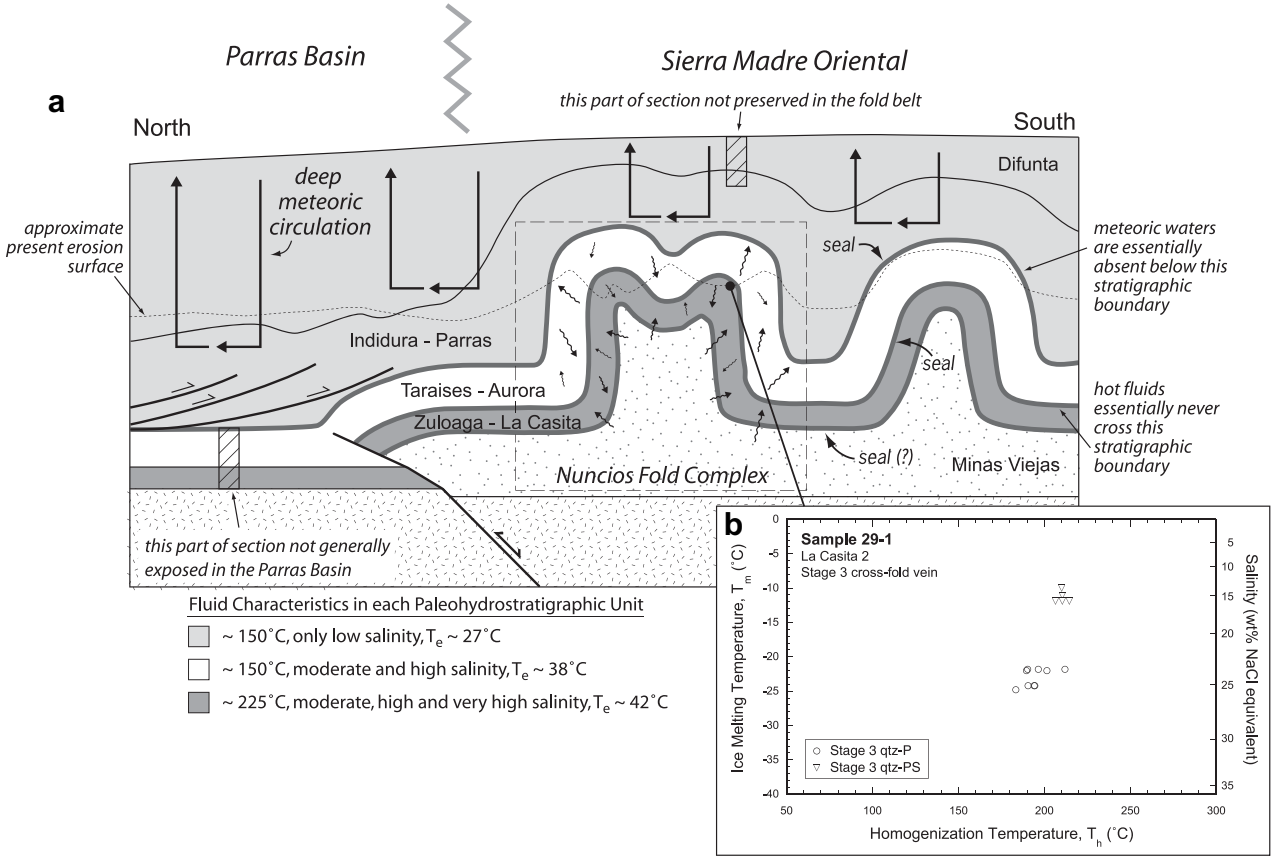

Fig. 19. (a) Schematic paleohydrologic model of the study area, including adjacent portions of the Parras Basin and Sierra Madre Oriental fold belt. System is reconstructed at the time of deposition of upper Difunta Group rocks (Fig. 3). Three seals, shown as heavy gray lines, vertically segregated the system into four paleohydrostratigraphic units, shown in white or grayscale shading. Fluids of differing salinity and temperature were present in each paleohydrostratigraphic unit. Repeated periodic communication occurred frequently within each unit and sometimes across regional seals as fold-related fractures formed, rapidly sealed and reopened multiple times. Note that uppermost Parras Shale and Difunta Group rocks were synchronously deposited with folding. Note also that although the deeper stratigraphy of the Parras Basin is poorly constrained, it is widely accepted that neither the Minas Viejas Fm. nor the San Juan Lentil of the Taraises Fm. exist there. (b) Fluid inclusion data from cross-fold vein sample 29-1. This is an example of a vein that preserves fluids with distinctly different salinities, but similar temperatures. As in Fig. 12, P and PS respectively refer to FIAs interpreted as primary or pseudosecondary.

Formations (Figs. 13b and 19a). In contrast, the Zuloaga and La Casita Formations comprised a lower paleohydrostratigraphic unit that contained moderate to very high salinity fluids that averaged near 225 °C, but ranged from 170 to 270 °C (Figs. 13c and 19a). Although the low salinity fluids were clearly sourced from the paleosurface, the moderate and high salinity brines most likely represent locally derived formation waters, whereas the highest salinity fluids were almost certainly sourced from the basal evaporites of the Minas Viejas Formation. Isotopic data presented by Lefticariu et al. (2005) support this interpretation for fluid sources.

Periodic connectivity of the paleohydrologic system is suggested by the multiple, distinctly different fluid salinities and T_h values preserved in many veins throughout the area (Figs. 13a and 19b), as well as the significant variations in fluid trapping pressures observed in some veins (e.g., Fig. 10). As fracturing occurred, fluids communicated more easily between formations in a given paleohydrostratigraphic unit (e.g., the Zuloaga and La Casita Fms.), and in some cases across regional seals (e.g., between the Taraises–Cupido unit and the Zuloaga–La Casita unit; Fig. 19a; Lefticariu et al., 2005). Variations in fluid advection rates and fracture sealing rates (e.g., Fig. 18) caused the preservation of multiple, distinctly different fluid salinities and temperatures in some veins (Fig. 19b), and the preservation of mixed, or intermediate fluid salinities and temperatures in others. We interpret the scatter in our data as a consequence of exactly these types of variations in fluid advection and fracture sealing rates, as well as the specific timing and location of vein formation. Although many veins were often reopened and hydrologically conductive during multiple fluid migration events, those events were limited in space and time because they occurred along complex, evolving, interconnected pathways. The creation, maintenance and destruction of these pathways were controlled by the spatio-temporal evolution of fracture networks that formed during folding (e.g., Laubach, 2003), which was in turn controlled by mechanical stratigraphy and fold kinematics (e.g., Fischer and Jackson, 1999; Hanks et al., 1997; Jamison, 1997).

Our results can be generalized for detachment folds that involve interlayered strong and weak lithotectonic units deforming largely by mesoscopic fracturing and forming at burial depths of 5–7 km. Fold-related fracturing will increase reservoir storativity and transmissivity, but only at relatively small scales (i.e., $<$100 m). A fold-related hydrologic system that begins as a series of many, small-scale reservoirs separated by thinner, hydrologically weaker seals (i.e., stacked pay), gradually evolves into a system with fewer, thicker, regional-scale reservoirs separated by excellent seals. These regional seals are likely to persist until the latest stages of folding where folds have steeper limb dips and smaller interlimb angles. At all times, fluid migration occurs in pulses whose location and duration are highly variable.

6. Conclusions

Abundant calcite and quartz veins in the Nuncios Fold Complex suggest that mesoscopic fractures played a significant role in the paleohydrology of this structure. Field and petrographic observations indicate that the veins are tectonic in origin, and formed in a general sequence that was related to progressive stages of folding. We collected samples from each stage of vein formation along a ~6 km transect across the fold, and used fluid inclusions to constrain the compositions and temperatures of the vein-forming fluids. We determined the structure and evolution of the paleohydrologic system by comparing fluid inclusion data from veins in different parts of the stratigraphic column, different structural positions and different vein stages. Our microthermometric data suggest that stratigraphy played the dominant role in controlling the structure of the paleohydrologic system, and that fluids in the NFC were partitioned into three regional hydrostratigraphic units. These units contained internally consistent T_h or salinity ranges, and the boundaries between them are marked by abrupt changes in T_h or salinity. No aspect of the data shows a recognizable change with time. Salinity and T_h do not correlate with vein stage, inclusion timing, or the relative timing of mineral precipitation. We interpret these characteristics as indicating periodic, local connectivity between formations or smaller-scale reservoirs that had slightly different and weakly segregated fluid compositions within regional paleohydrostratigraphic units, but a general persistence of the stratigraphic seals that separated the regional units.

The unique timing and location of fracturing and sealing in a detachment fold can lead to a complex regional hydrologic system comprising a stratigraphic and/or structural partitioning of fluids, and numerous, discrete, fluid migration events. As a result, any individual vein in a detachment fold may have a complex, unique, hydrologic history. The same can be said for hydrologic systems that show outcrop-scale heterogeneity. Although one might be able to determine detailed, consistent timing and filling relationships at one outcrop, veins in another outcrop a few kilometers away may display a very different timing and filling history. Consequently, in areas where regional paleohydrologic systems are heterogeneous, care must be taken when interpreting data collected from veins in only one stratigraphic or lithologic unit, structural position or small geographic location. Although outcrop and individual vein data will reflect the characteristics of local fluid-rock interactions, they may not reproduce the overall spatio-temporal heterogeneity of regional paleohydrologic systems.

Acknowledgments

This research was funded by NSF grant EAR-9972993 to Fischer and Perry, and by student research grants to Higuera-Diaz and Lefticariu from AAPG, GSA, and the Goldich Fund of the NIU Department of Geology and Environmental Geosciences. We thank Steve Laubach and Charlie Onasch for thorough and insightful reviews that significantly improved the clarity of the manuscript. Bob Holdsworth did an admirable job of trying to teach us the Queen's English, for which we are also grateful.

Appendix. Supplementary data

Supplementary data associated with this article can be found, in the online version, at doi:10.1016/j.jsg.2009.09.004.

References

Bethke, C.M., Marshak, S., 1990. Brine migration across North America – the plate tectonics of groundwater. Annual Review of Earth and Planetary Science 18, 287–315.

Bodnar, R.J., 1992. Revised equation and table for freezing point depressions of H_2O-salt fluid inclusions (abs). In: PACROFI IV, Fourth Biennial Pan-American Conference on Research on Fluid Inclusions, Program and Abstracts, Lake Arrowhead, CA, vol. 14, p. 15.

Brantley, S.L., Fisher, D.M., Deines, P., Clark, M.B., Myers, G., 1997. Segregation veins: evidence for the deformation and dewatering of a low-grade metapelite. In: Holness, M.B. (Ed.), Deformation-enhanced Fluid Transport in the Earth's Crust and Mantle. Chapman and Hall, London, pp. 267–288.

Cosgrove, J.W., 1993. The interplay between fluids, folds, and thrusts during the deformation of a sedimentary succession. Journal of Structural Geology 15, 491–500.

Crawford, M.L., 1981. Phase equilibria in aqueous fluid inclusions. In: Hollister, L.S., Crawford, M.L. (Eds.), Short Course in Fluid Inclusions: Applications to Petrology. Short Course Handbook, vol. 6. Mineralogical Association of Canada, pp. 75–100.

Dahlstrom, C.D.A., 1990. Geometric constraints derived from the law of conservation of volume and applied to evolutionary models for detachment folding. American Association of Petroleum Geologists Bulletin 74, 336–344.

Dieterich, D., McKenzie, J.A., Song, H., 1983. Origin of calcite in syntectonic veins as determined from carbon-isotope ratios. Geology 11, 547–551.

Dorobek, S., 1989. Migration of orogenic fluids through Siluro-Devonian Helderberg Group during late Paleozoic deformation: constraints on fluid sources and implications for thermal histories of sedimentary basins. Tectonophysics 159, 24–45.

Duan, Z., Møller, N., Weare, J.H., 1992a. An equation of state for the CH_4–CO_2–H_2O system I. Pure systems from 0 to 1000 °C and 0 to 8000 bar. Geochimica et Cosmochimica Acta 56, 2605–2617.

Duan, Z., Møller, N., Weare, J.H., 1992b. An equation of state for the CH_4–CO_2–H_2O system II. Mixtures from 50 to 1000 °C and 0 to 1000 bar. Geochimica et Cosmochimica Acta 56, 2619–2631.

Epard, J.-L., Groshong, R.H., 1995. Kinematic model of detachment folding including limb rotation, fixed hinges and layer-parallel strain. Tectonophysics 247, 85–103.

Evans, M.A., Battles, D.A., 1999. Fluid inclusion and stable isotope analyses of veins from the central Appalachian Valley and Ridge province: implications for regional synorogenic hydrologic structure and fluid migration. Geological Society of America Bulletin 111 (12), 1841–1860.

Fischer, M.P., Jackson, P.B., 1999. Stratigraphic controls on deformation patterns in fault-related folds: a detachment fold example from the Sierra Madre Oriental, northeast Mexico. Journal of Structural Geology 21, 613–633.

Fyfe, W.S., Kerrich, R., 1985. Fluids and thrusting. Chemical Geology 49 (1-3), 353–362.

Gale, J.F.W., Gomez, L.A., 2007. Late opening-mode fractures in karst-brecciated dolostones of the Lower Ordovician Ellenburger Group, west Texas: recognition, characterization, and implications for fluid flow. American Association of Petroleum Geologists Bulletin 91 (7), 1005–1023.

Garvin, G., 1995. Continental-scale groundwater flow and geological processes. Annual Reviews of Earth and Planetary Sciences 24, 89–117.

Giles, K.A., Lawton, T.F., 1999. Attributes and evolution of an exhumed salt weld, La Popa basin, northeastern Mexico. Geology 27 (4), 323–326.

Goldhammer, R.K., 1999. Mesozoic sequence stratigraphy and paleogeographic evolution of northeast Mexico. In: Bartolini, C., Wilson, J.L., Lawton, T.F. (Eds.), Mesozoic Sedimentary and Tectonic History of North-Central Mexico. Geological Society of America, pp. 1–58. Special Paper 340.

Goldhammer, R.K., Lehman, P.J., Todd, R.G., Wilson, J.L., Ward, W.C., Johnson, C.R., 1991. Sequence Stratigraphy and Cyclostratigraphy of the Mesozoic of the Sierra Madre Oriental, Northeast Mexico, A Field Guidebook. Society of Economic Paleontologists and Mineralogists, Gulf Coast Section, 85 p.

Goldstein, R.H., Reynolds, T.J., 1994. Systematics of fluid inclusions in diagenetic minerals. In: SEPM Short Course, vol. 31, 199 p.

Gray, D.R., Gregory, R.T., Durney, D.W., 1991. Rock-buffered fluid-rock interaction in deformed quartz-rich turbidite sequences, eastern Australia. Journal of Geophysical Research 96, 19681–19704.

Haas, J.A., 1978. An empirical equation with tables of smoothed solubilities of methane in water and aqueous sodium chloride solutions up to 25 weight percent 360 degrees C, and 138 MPa. United States Geological Survey Open File Report 78-1004, 42 p.

Hanks, C.L., Lorenz, J., Teufel, L., Krumhardt, A.P., 1997. Lithologic and structural controls on natural fracture distribution and behavior within the Lisburne Group, northeastern Brooks Range and North Slope subsurface, Alaska. American Association of Petroleum Geologists Bulletin 81 (10), 1700–1720.

Hanks, C.L., Parris, T.M., Wallace, W.K., 2006. Fracture paragenesis and microthermometry in Lisburne Group detachment folds: implications for the thermal and structural evolution of the northeastern Brooks Range, Alaska. American Association of Petroleum Geologists Bulletin 90 (1), 1–20.

Hanor, J.S., 1980. Dissolved methane in sedimentary brines: potential effect on PVT properties of fluid inclusions. Economic Geology 75, 603–609.

Higuera-Diaz, I.C., 2005. Geometry, kinematics, and paleofluid systems of a detachment fold complex in northeastern Mexico. Unpublished MS thesis, Northern Illinois University, DeKalb, Illinois, 135 p.

Higuera-Diaz, I.C., Fischer, M.P., Wilkerson, M.S., 2005. Geometry and kinematics of the Nuncios detachment fold complex: implications for lithotectonics in northeastern Mexico. Tectonics 24 (4), TC4010. doi:10.1029/2003TC001615.

Holland, R.A.G., Bray, C.J., Spooner, E.T.C., 1978. A method for preparing doubly polished thin sections suitable for microthermometric examination of fluid inclusions. Mineralogical Magazine 42, 407–408.

Homza, T.X., Wallace, W.K., 1995. Geometric and kinematic models for detachment folds with fixed and variable detachment depths. Journal of Structural Geology 17, 575–588.

Jamison, W.R., 1997. Quantitative evaluation of fractures on Monkshood Anticline, a detachment fold in the foothills of Western Canada. American Association of Petroleum Geologists Bulletin 81 (7), 1110–1132.

Janssen, C., 1998. Fluid regime in faulting deformation of the Waratah Fault Zone, Australia, as inferred from major and minor element analyses and stable isotopic signatures. Tectonophysics 294 (1–2), 109–130.

Kirschner, D.L., Sharp, Z.D., Teyssier, C., 1993. Vein growth mechanisms and fluid sources revealed by oxygen isotope laser microprobe. Geology 21, 85–88.

Kirschner, D.L., Teyssier, C., Gregory, R.T., Sharp, Z.D., 1995. Effect of deformation on oxygen isotope exchange in the Heavitree Quartzite, Ruby Gap duplex, central Australia. Journal of Structural Geology 17 (10), 1407–1423.

Kisch, H.J., van den Kerkhof, A.M., 1991. CH_4-rich inclusions from quartz veins in the Valley-and-Ridge Province and the anthracite fields of the Pennsylvania Appalachians. American Mineralogist 76 (1–2), 230–240.

Laubach, S.E., 1988. Fractures generated during folding of the Palmerton Sandstone, eastern Pennsylvania. Journal of Geology 96, 495–503.

Laubach, S.E., 2003. Practical approaches to identifying sealed and open fractures. American Association of Petroleum Geologists Bulletin 87 (4), 561–579.

Laudon, R.C., 1984. Evaporite diapirs in the La Popa Basin, Nuevo Leon, Mexico. Geological Society of America Bulletin 95 (10), 1219–1225.

Lawler, J.P., Crawford, M.L., 1983. Stretching of fluid inclusions resulting from a low-temperature microthermometric technique. Economic Geology 78, 527–529.

Lefticariu, L., Perry, E.C., Fischer, M.P., Banner, J.L., 2005. Sources and timing of fluids in an evaporite-detached fold complex: stable and radiogenic isotope constraints. Geology 33 (1), 69–72,. doi:10.1130/G20592.1.

Le Pichon, X., Kobayashi, K., Kaiko-Nankai, 1992. Fluid venting activity within the eastern Nankai trough accretionary wedge: a summary of the 1989 Kaiko-Nankai results. Earth and Planetary Science Letters 109 (3–4), 303–318.

Marrett, R., Aranda-Garcia, M., 1999. Structure and kinematic development of the Sierra Madre Oriental fold-thrust belt, Mexico. In: Marrett, R., Wilson, J.L., Ward, W.C. (Eds.), Stratigraphy and Structure of the Jurassic and Cretaceous Platform and Basin Systems of the Sierra Madre Oriental, Monterry and Saltillo areas, northeast Mexico: A Field Book and Related Papers. South Texas Geological Society, pp. 69–98.

Marrett, R., Laubach, S.E., 2001. Fracturing during burial diagenesis. In: Marrett, R. (Ed.), Genesis and Controls of Reservoir-scale Carbonate Deformation, Monterrey Salient, Mexico Guidebook, vol. 28. Bureau of Economic Geology, University of Texas at Austin, pp. 109–122.

McBride, E.F., Weidie, A.E., Wollenben, J.A., Laudon, R.C., 1974. Stratigraphy and structure of the Parras and La Popa Basin, northeastern Mexico. Geological Society of America Bulletin 85, 1603–1622.

Meunier, J.D., 1989. Assessment of low-temperature fluid inclusions in calcite using microthermometry. Economic Geology 84, 167–170.

Mitra, S., 2003. A unified kinematic model for the evolution of detachment folds. Journal of Structural Geology 25 (10), 1659–1673.

Monroy-Santiago, F., Laubach, S.E., Marrett, R., 2001. Preliminary diagenetic and stable isotope analyses of fractures in the Cupido Formation, Sierra Madre Oriental. In: Marrett, R. (Ed.), Genesis and Controls of Reservoir-scale Carbonate Deformation, Monterrey Salient, Mexico Guidebook, vol. 28. Bureau of Economic Geology, University of Texas at Austin, pp. 83–107.

Mullis, J., 1987. Fluid inclusion studies during very low-grade metamorphism. In: Frey, M. (Ed.), Low Temperature Metamorphism. Blackie, London, pp. 162–199.

Nesbitt, B.E., Muehlenbachs, K., 1994. Paleohydrology of the Canadian Rockies and origin of brines, Pb–Zn deposits and dolomitization in the Western Canada Sedimentary Basin. Geology 22, 243–246.

Odling, N.E., Gillespie, P., Bourgine, B., Castaing, C., Chilés, J.-P., Christensen, N.P., Fillion, E., Genter, A., Olsen, C., Thrane, L., Trice, R., Aarseth, E., Walsh, J.J., Watterson, J., 1999. Variations in fracture system geometry and their implications for fluid flow in fractured hydrocarbon reservoirs. Petroleum Geoscience 5, 373–384.

Oliver, J., 1986. Fluids expelled tectonically from orogenic belts: their role in hydrocarbon migration and other geologic phenomena. Geology 14, 99–102.

Oliver, N.H.S., Cartwright, I., Wall, V.J., Golding, S.D., 1993. The stable isotope signature of kilometre-scale fracture-dominated metamorphic fluid pathways, Mary Kathleen, Australia. Journal of Metamorphic Geology 11 (5), 705–720.

Ortega, O., Marrett, R., 2001. Stratigraphic controls on fracture intensity in Barremian–Aptian carbonates, northeastern Mexico, in. In: Marrett, R. (Ed.), Genesis and Controls of Reservoir-scale Carbonate Deformation, Monterrey Salient, Mexico. Guidebook No. 28. Bureau of Economic Geology, University of Texas at Austin, pp. 83–107.

Padilla y Sanchez, R., 1982. Geologic evolution of the Sierra Madre Oriental between Linares, concepcion del Oro, Saltillo, and Monterrey, Mexico. Ph.D. thesis, University of Texas at Austin, Austin, Texas, 217 p.

Poblet, J., McClay, K., 1996. Geometry and kinematics of single-layer detachment folds. American Association of Petroleum Geologists Bulletin 80, 1085–1109.

Richards, I., Connelly, J.B., Gregory, R.T., Gray, D.R., 2002. The importance of diffusion, advection, and host-rock lithology on vein formation: a stable isotope study from the Paleozoic Ouachita orogenic belt, Arkansas and Oklahoma. Geological Society of America Bulletin 114 (11), 1343–1355.

Roedder, E., 1973. The composition of fluid inclusions. U.S. Geological Survey Professional Paper 440-JJ, 164 p.

Rowan, M.G., 1997. Three-dimensional geometry and evolution of a segmented detachment fold, Mississippi Fan foldbelt, Gulf of Mexico. Journal of Structural Geology 19 (3–4), 463–480.

Rye, D.M., Bradbury, H.J., 1988. Fluid flow in the crust: an example from a Pyrenean thrust ramp. American Journal of Science 288, 197–235.

Shepherd, T.J., Rankin, A.H., Alderton, D.H.M., 1985. A Practical Guide to Fluid Inclusion Studies. Blackie, Glasgow, 239 p.

Sibson, R.H., 1996. Structural permeability of fluid-driven fault-fracture meshes. Journal of Structural Geology 18 (8), 1031–1042.

Sterner, S.M., Hall, D.L., Bodnar, R.J., 1988. Synthetic fluid inclusions. V. Solubility relations in the system NaCl–KCl–H_2O under vapor-saturated conditions. Geochimica et Cosmochimica Acta 52, 989–1005.

Touret, J.L.R., 2001. Fluids in metamorphic rocks. Lithos 55 (1–4), 1–25.

Travé, A., Calvet, F., Sans, M., Vergés, J., Thirlwall, M., 2000. Fluid history related to the Alpine compression at the margin of the south-Pyrenean Foreland basin: the El Guix anticline. Tectonophysics 321, 73–102.

van den Kerkhof, A.M., 1988. Phase transitions and molar volumes of CO_2–CH_4–N_2 inclusions. Bulletin Minéralogique 111, 257–266.

van den Kerkhof, A.M., 1990. Isochore phase diagrams in the systems CO_2–CH_4 and CO_2–N_2: application to fluid inclusions. Geochimica et Cosmochimica Acta 54, 261–269.

Vrolijk, P., 1987. Tectonically driven fluid flow in the Kodiak accretionary complex, Alaska. Geology 15, 466–469.

Wall, J.R., Murray, G.E., Diaz, T., 1961. Geologic occurrence of intrusive gypsum and its effect on structural forms in Coahuila Marginal Folded Province of northeastern Mexico. American Association of Petroluem Geologists Bulletin 45, 1504–1522.
Wickham, S.M., Peters, M.T., Fricke, H.C., O'Neil, J.R., 1993. Identification of magmatic and meteoric fluid sources and upward- and downward-moving infiltration fronts in a metamorphic core complex. Geology 21, 81–84.
Weidie, A.E., Martinez, J.D., 1970. Evidence for evaporite diapirism in northeastern Mexico. American Association of Petroleum Geologists Bulletin 54, 655–661.
Wilson, J.L., Ward, W.C., Finneran, J.M., 1984. A Field Guide to Upper Jurassic and Lower Cretaceous Carbonate Platform and Basin Systems Monterrey-Saltillo Area, Northeast Mexico. Society of Economic Paleontologists and Mineralogists, Gulf Coast Section, San Antonio, TX, 76 p.